metals

MDPI

Review

Processing and Properties of Reversion-Treated Austenitic Stainless Steels

Antti Järvenpää [1,*], Matias Jaskari [1], Anna Kisko [2] and Pentti Karjalainen [2]

[1] Kerttu Saalasti Institute, University of Oulu, FI-85500 Nivala, Finland; matias.jaskari@oulu.fi
[2] Centre for Advanced Steels Research, University of Oulu, FI-90014 Oulu, Finland; anna.kisko@oulu.fi (A.K.); pentti.karjalainen@oulu.fi (P.K.)
* Correspondence: antti.jarvenpaa@oulu.fi; Tel.: +35-844-555-1633

Received: 6 December 2019; Accepted: 18 February 2020; Published: 21 February 2020

Abstract: Strength properties of annealed austenitic stainless steels are relatively low and therefore improvements are desired for constructional applications. The reversion of deformation induced martensite to fine-grained austenite has been found to be an efficient method to increase significantly the yield strength of metastable austenitic stainless steels without impairing much their ductility. Research has been conducted during thirty years in many research groups so that the features of the reversion process and enhanced properties are reported in numerous papers. This review covers the main variables and phenomena during the reversion processing and lists the static and dynamic mechanical properties obtained in laboratory experiments, highlighting them to exceed those of temper rolled sheets. Moreover, formability, weldability and corrosion resistant aspects are discussed and finally the advantage of refined grain structure for medical applications is stated. The reversion process has been utilized industrially in a very limited extent, but apparently, it could provide a feasible processing route for strengthened austenitic stainless steels.

Keywords: metastable austenitic stainless steel; cold rolling; annealing; reversion; grain size; mechanical properties; fatigue; corrosion; medical applications

1. Background

Austenitic stainless steels (ASSs) are potential candidates for structural parts in transportation and construction industries due to their excellent formability, work hardening capability and weldability, together with good corrosion resistance. However, their yield strength (YS) is generally low, for instance for the EN 1.4301/AISI 304 around 210–230 MPa and 330–350 MPa for EN 1.4318/AISI 301LN grade [1], which limits their use for structural applications. (For the ASSs grades, AISI codes will be used hereafter as commonly in the literature). Many grades are, however, metastable at room temperature, which means that the austenite phase transforms to martensite during cold working, so that their work hardening capability and ductility can be utilized to improve the strength by cold deformation (the temper rolling process). As an example, the strengthened condition +C1000 with the minimum proof strength ($R_{p0.2}$) of 700 MPa [2] can be achieved by about a 20% cold rolling thickness reduction for 304 and 301LN ASSs, with some loss of elongation. However, the disadvantage of strengthening by temper rolling is the formation of anisotropy in mechanical properties, the strength being different in different directions relative to the rolling direction [3,4]. Moreover, lowest values are obtained in compression tests parallel to the rolling direction [3]. The cold rolling tends also to impair the corrosion resistance of ASSs [5–7].

The strength of ASSs can also be increased by nitrogen alloying, and the processing and properties of high-nitrogen steels have been investigated extensively, e.g., [8,9]. However, in conventional

processing of Cr-Ni alloys, the limit of nitrogen solubility is low and problems with the hot ductility may also appear with increased nitrogen content [4]. Hence, other strengthening methods are desirable.

Grain size (GS) refinement is an effective method for increasing the static strength properties of metals and alloys (the Hall–Petch relationship) and also their fatigue performance, especially in the high-cycle fatigue (HCF) regime. The GS of commercial ASSs is typically larger than 10 μm. Even though the impact of GS on strength is not so high in ASSs as in ferritic steels, it has been shown in a large number of papers that the refinement of GS can provide significant improvement in the YS of austenite, e.g., [10–29]. The traditional hot rolling process or cold rolling and recrystallization annealing are not effective for refining the GS of the austenite phase, although GS of 2 μm has been obtained by using warm rolling and annealing [30]. The role of dynamic recrystallization in GS refinement in ASSs has been reviewed by Zhao and Jiang [31], but it is not very efficient due to high temperatures required. However, the reversion treatment, in which deformation-induced α'-martensite (DIM) transforms back to austenite has been shown to refine the austenite GS to submicron size, resulting in excellent combinations of YS and tensile elongation (TE), as reported in numerous studies during the last 30 years.

The martensite to austenite reversion process in austenitic Cr-Ni steels was already studied in the 1970s and 1980s [32–37], but it continued comprehensively in Japan in early 1990s, e.g., [38–40] and later in many groups in various countries, e.g., [10–21,30,41–79]. The studies in Finland, starting in 2004, as supported by a Finnish stainless-steel company and in collaboration with two research groups in USA and one in the Czech Republic, may be mentioned separately [22–29,80–103]. In laboratory studies, the reversion process has been applied to several commercial Cr-Mn and Cr-Ni steel grades such as 201, 201L, 204Cu, 301, 301LN, 304, 304L (see later in Section 5.1).

As the reversion process is carried out simply using cold rolling and annealing, it seems more appropriate for bulk production of large-sized sheets and has more potential for actual applications than numerous other severe plastic deformation techniques applied to GS refinement. However, despite extensive academic research work, as far as the present authors know, there only exist a couple of industrial companies utilizing the reversion-treatment for ASSs. In Japan, Nano grains Co. Ltd (Komatsuseiki Kosakusho Co., Ltd.) produces grain-refined 304, 316 and 301 foils (thickness range 80–300 μm), with the GS finer than 1 μm, using repeated reversion treatment [104]. Especially the enhanced properties of micro-scale cutting and hole piercing are utilized in the manufacturing of orifices for electronic fuel injection [105–107]. Nippon Steel & Sumitomo Metal company lists in its product catalogue fine-grained 304 (SUS304 BA19) and 301L (NSSMC-NAR-301L BA1) grades: thin sheets, strips and foils (0.08–0.6 mm) having both high strength, ductility and formability and smooth formed surface due to refinement of GS [108,109]. The feasibility of the process for an industrial manufacturing using a continuous annealing line has been demonstrated in one laboratory study [12]. In recent studies by Järvenpää et al. [87], a pilot induction heating line has been employed to simulate industrial conditions in reversion annealing of the 301LN grade.

In order to highlight the advantages of grain-refined ASSs, in the present paper, the main process variables and their influences in the reversion-treatment are introduced, and the state of the art of mechanical properties of reversion-treated, fine-grained ASSs are reviewed. The formability, weldability, corrosion properties and medical applications are also included in this survey. A short overview of the state of the research on the reversion process has recently been published as a conference paper [103], but the present review is much more comprehensive than that.

2. Cold Rolling Stage

The first stage of the reversion treatment is cold rolling of an ASS sheet to obtain DIM, which can be reversed to fine-grained austenite in the subsequent annealing stage. In the following, we point out the different stability of the austenite in different ASSs towards transforming to martensite, depending mainly on the chemical composition of the steel. Some commercial ASS grades will be compared. The degree of cold rolling reduction is a factor affecting the fraction of DIM created,

and in industrial rolling, it cannot very high. Therefore, only partial transformation of austenite to DIM can happen affecting the microstructure obtained in the annealing stage. Further, the DIM forming gradually will be inevitably deformed to different degrees, which also has an influence on microstructure heterogeneity and thereby on the mechanical properties.

The reversion heat treatment for ASSs consisting of the cold rolling and annealing stages is schematically presented in Figure 1. A metastable ASS must first be cold worked to transform the austenite to DIM and deform it. There is often some hexagonal ε-martensite formed as well, but its fraction and contribution are minor in the reversion process, so that much attention has not been paid on that phase. Highly-deformed cell-type DIM is preferable for a source of a large number of nucleation sites for new austenite grains to attain the desired highly-refined GS in the subsequent reversion annealing [38–40]. If the total cold-rolling reduction is small, the transformation of austenite to DIM tends to remain partial and coarse-grained deformed austenite (DA) grains are retained in the structure. Furthermore, the lath-type, slightly deformed DIM reverses into austenite with coarser GS. Accordingly, very high cold rolling reductions of 90% to 95% were recommended originally and applied in numerous studies, e.g., [14,15,17,19,20,39,40], which can, however, be impractical in industry.

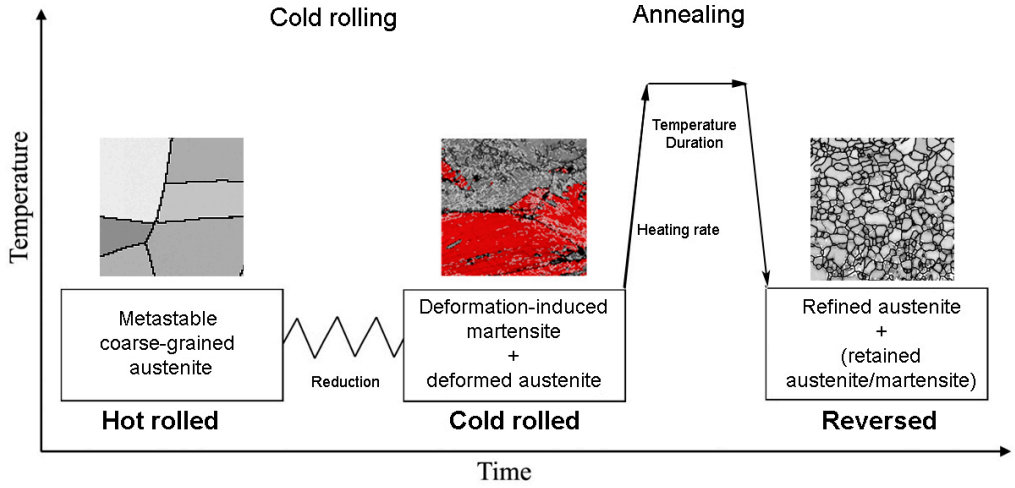

Figure 1. Reversion treatment of a metastable austenitic stainless-steel consisting of cold rolling and annealing stages. Important variables have been designated.

The austenite thermal stability has been discussed by Lo et al. [110] in their extensive review on ASSs, listing numerous Equations for the chemical compositional dependence of M_s temperature, for instance. The mechanical stability, the susceptibility of austenite to DIM formation, is mainly affected by the chemical composition of the steel and its GS, but also GS distribution, grain morphology and orientation as well as deformation conditions (stress state, temperature, pass strains, strain rate, etc.) have their influence [111,112]. Das et al. [113] have collected a very extensive literature data and developed a neural network model to predict the amount of DIM formation with its influencing parameters in a variety of ASSs. Mechanical driving force (stress) and temperature were found to have high significance, while concerning uniaxial tensile testing conditions. Regarding GS refinement, highly metastable grades are favored, and according to Tomimura et al. [38], the Ni equivalent (Ni + 0.35Cr) ≤ 16.0% (all compositions are in mass %) is required to transform more than 90% of austenite to DIM during 90% cold rolling at room temperature (RT).

The Nohara equation (Equation (1)), defining the temperature at which the amount of 50% DIM is transformed from austenite through cold deformation of 0.30 true strain, is commonly used for evaluation of the mechanical stability of austenite in rolling [114]. It shows that all alloying elements decrease the stability, though with varying power.

$$M_{d30}\ (^{\circ}C) = 552 - 462(C + N) - 9.2Si - 8.1Mn - 13.7Cr - 29(Ni + Cu) - 18.5Mo - 68Nb - 1.42(GS - 8) \quad (1)$$

Here the alloying elements are in mass % and GS is in ASTM unit. The M_{d30} temperature is around 20–40 °C for 301LN, whereas lower for 304 (examples in Table 1). From Equation (1), it is also seen that during deformation Ni stabilizes austenite more than Mn does, which is contrary to that concerning thermodynamic austenite stability [115]. Refining the GS also increases the stability, as reported in numerous studies, e.g., [46,75,114]. In repeated reversion treatments, to be discussed shortly later, this means that in subsequent cold rolling stages, the DIM formation becomes reduced [21]. The relationship between austenite GS and its stability under tensile and fatigue loading will be discussed later in Section 5.

In addition to alloying adjustments, another method to enhance the DIM transformation is rolling at lowered temperatures, the technique which has been applied to 304/304L and 316L grades in particular [10,41,66,116–120].

To give examples, the DIM fractions formed during cold rolling for some Cr-Mn and Cr-Ni ASSs (the exact chemical compositions are listed in Table 1; concentrations are always in mass %) are plotted as a function of the cold rolling thickness reduction in Figure 2. They show that in the 304/304L grade, only a small fraction of DIM can be obtained at RT [20,121]. After a 90% cold rolling reduction, Di Schino et al. [11] obtained 35% and Ravi Kumar et al. [54] 43% of DIM. However, at 0 °C, in experiments performed by Forouzan et al. [14], about 55% DIM was formed by a 30% cold rolling reduction in a 304 ASS (M_{d30} = 13 °C), and even a completely martensitic structure could be obtained after 60% reduction. In a 301LN ASS (M_{d30} ≈ 23–27 °C) in order to achieve a fully martensitic structure, a cold rolling reduction of about 60% is required [23,29,102], but for 201 and 201L grades, the reduction of 40% can be enough for that [15,16,67]. However, it must be noted that for this higher metastability of 201/201L ASSs, the nitrogen content must be low, for in experiments performed by Kisko et al. [28,83,101] and Hamada et al. [80] using the 201 grade with 0.052%C and 0.245%N, the DIM fraction obtained was only 30% after 60% cold rolling reduction. Hence, the exact chemical composition can greatly affect the mechanical stability which can vary within an ASS grade, requiring attention. As seen from Figure 2, if single pass reductions are high, adiabatic heating tends to reduce markedly the extent of DIM formed [4,77].

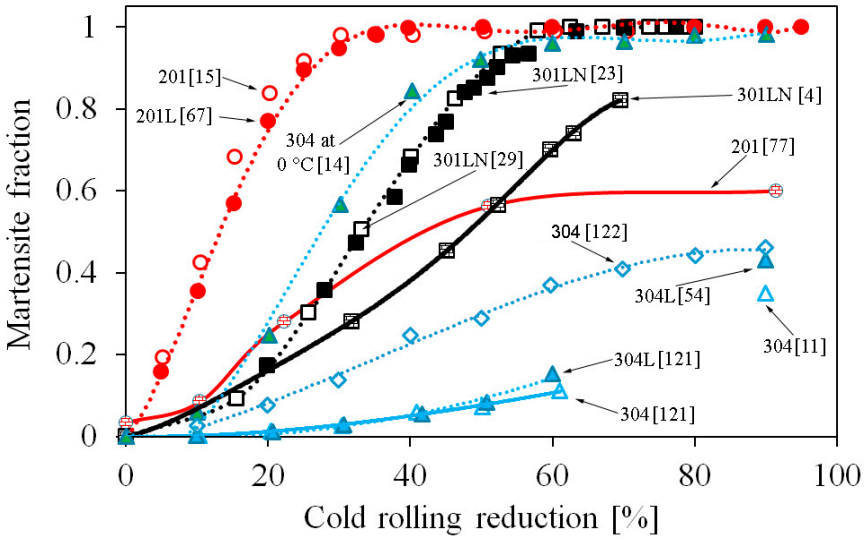

Figure 2. Examples of increase of the deformation-induced martensite fraction during cold rolling deformation in 201/201L, 304/304L and 301LN grades. The chemical compositions of the steels are in Table 1.

Mirzadeh and Najafizadeh [122] have modeled by means of an artificial neural network the effect of the cold working temperature, amount of deformation, strain rate and initial austenite GS on the volume fraction of DIM in a 301LN ASS. The appropriate grain refining zone can be determined

using this model. The martensite content is increased when the degree of deformation is high or the deformation temperature is low. Moreover, by increasing the strain rate and the ASTM GS number (i.e., refining the GS), the amount of DIM is reduced.

Table 1. Chemical compositions and Md_{30} temperatures for Austenitic stainless steels (ASSs) in Figure 2.

Grade	C	Si	Mn	Cr	Ni	Mo	N	M_{d30}	Ref.
201	0.080	0.54	5.90	16.60	3.70	0.11	0.040		[15]
201	0.024	0.38	7.02	17.06	4.07	0.04	0.164		[77]
201L	0.027	0.51	5.91	16.20	3.88	0.08	0.040		[67]
301LN	0.017	0.52	1.29	17.30	6.50	0.15	0.150	27	[23]
301LN	0.025	0.53	1.25	17.50	6.50	0.09	0.150	23	[29]
301LN	0.024	0.54	1.22	17.80	6.40		0.133	28	[4]
304	0.040	0.34	1.15	18.06	8.33	0.05	0.048	6.2	[123]
304	0.060	0.02	0.33	18.40	8.60	0.06	0.024	9.6	[11]
304	0.065	0.48	1.35	18.20	8.37		0.046	−6.7	[121]
304L	0.021	0.56	1.37	18.44	9.38		0.038	−16	[121]
304L	0.027	0.43	1.58	18.20	8.22	0.35		13	[14]
304L	0.020	0.30	1.50	18.60	10.10		0.020	−29	[54]

Concerning the actual deformation degree experienced by DIM during cold rolling, it is important to realize that the DIM formation proceeds gradually, as seen in Figure 2. This means that at low rolling reductions, a significant fraction of the formed DIM remains inevitably only "slightly-deformed" and the resultant lath martensite plays a significant role in the microstructure evolution. In industrial practice, however, heavy cold rolling or complex processing routes are not desired. Promisingly, for instance for a 301LN ASS, cold rolling reductions as low as 35% to 52% seem to result in excellent strength-ductility combinations (see Table 2 in Section 5.1), even though the GS refinement is not most efficient and the GS obtained is not uniform [23,29]. Even very low reductions such as 10% to 40% have been reported to reduce significantly the average GS in 301LN during complete reversion [60,64].

The stability of austenite under tensile deformation will be further discussed in Section 5. It can be mentioned here that Ahmedabadi et al. [124] have recently modelled the DIM formation ($f_{\alpha'}$) during cold rolling of a 304 ASS using a sigmoidal logistic equation, Equation (2):

$$f_{\alpha'} = \frac{f_s}{1 + exp[-\beta(\varepsilon - \varepsilon_m)]} \quad (2)$$

In the equation, the parameter f_s is the maximum value of a given "S"-curve, ε_m is the abscissa of the mid-point of a given sigmoid, and ε is deformation strain. The parameter β represents the steepness of the curve. The fitting parameters for the model can be correlated to physical parameters associated with the austenite to DIM transformation. This model eliminates the limitations present in the previous models, as discussed. Importantly it shows that it is not always possible to completely transform austenite into martensite, which means that the DA affects the microstructure evolution in reversion annealing.

3. Reversion Annealing

During the annealing stage of the cold-rolled ASS sheet containing DIM, the reversion of DIM back to austenite can take place, refining the GS and enhancing the mechanical properties. There are two reversion mechanisms, shear and diffusional ones, the type depending on the chemical composition of the steel, heating rate and annealing temperature but hardly on the degree of cold rolling reduction. In this chapter, we first discuss the type and kinetics of the reversion in various Cr-Ni type ASSs and the factors affecting them. This section is followed by the discussion on the temperature range suitable for the reversion treatment, accounting for the different reversion mechanism. It can be noticed that certain typical temperatures (600–1000 °C) have been applied in experiments for commercial Cr-Ni

and Cr-Mn ASSs, and the duration of annealing can be selected to be very short (less than 1 s) or even hours, highlighting the flexibility of the process.

3.1. Reversion Mechanism

In metastable ASSs, DIM reverses back to austenite during continuous heating or isothermal annealing at an appropriate temperature regime. Reversion of martensite to austenite is a phenomenon also taking place during intercritical annealing in low carbon martensitic stainless steels [125] and medium-Mn steels, e.g., [126]. A variety of experimental methods have been employed to study both martensitic transformation and DIM reversion in ASSs, e.g., microscopic methods, dilatometry, calorimetry, X-ray diffraction (both postmortem and in situ), internal friction, various magnetic, positron annihilation or hardness/mechanical properties measurements [127–132]. A small amount of ε-martensite can form in some ASSs at small deformation degrees, and it reverses at much lower temperatures than α′-martensite does (see e.g., [63]). Singh [37] reported that the ε-martensite was stable up to 200 °C, and according to Santos and Andrade [128], it reverses in the temperature range 50–200 °C and between 150–400 °C according to Dryzek et al. [129]. Very recently a latent strengthening mechanism, bake hardening without interstitials, due to the reversion of ε-martensite, has been reported in a metastable FCC high entropy alloy by Wei et al. [133]. Annealing for 20 min at 200 °C was enough for complete reversion accomplished by a shear-assisted displacive mechanism.

The reversion of α′-martensite (i.e., DIM) to austenite can occur by two different mechanisms, a diffusionless shear or diffusion-controlled one, as reported already in 1967 by Guy et al. [36]; see also [39,45]. Guy et al. observed that austenite with mechanical twins formed first from martensite in 18Cr-8Ni and 18Cr-12Ni steels, which then recovered to a subgrain structure. Concerning the GS refinement, both reversion mechanisms can readily lead to a micron-scale GS, though in principle the diffusional reversion is more efficient [38]. In Fe-Cr-Ni ternary alloys, in the first stage, the shear phase reversion results in austenite which contains traces of prior α′-martensite morphology, the same grain boundaries as those of original austenite and a high density of defects. After the fast transformation, defect-free austenite subgrains are formed which coalesce to a structure resembling recrystallized structure [38,39]. An example of the formation of dislocation free grains from subgrains is shown in Figure 3a. On the contrary, the diffusional reversion is characterized by the nucleation and growth of randomly oriented equiaxed austenite grains; the result is shown in Figure 3b. The nucleation occurs on the cell or lath boundaries of the deformed DIM, and austenitic grains grow in size with time but can stay in a nanometer or submicron range. Secondary phase precipitates can also form in the course of the reversion, for instance nano-size chromium nitrides in 301LN [22,26,89] (Figure 3c,d) and carbides in 301 [130,134,135].

The chemical composition of the steel and annealing temperature are two important variables affecting the type of the reversion mechanism [23,39]. Tomimura and co-workers [39] reported that the reverse transformation of martensite to austenite occurs by diffusionless mechanism in metastable Fe–Cr–Ni ternary alloys with the high ratio of Ni to Cr (about ≥0.6), whereas the diffusive reverse transformation happens at the low ratio of Ni to Cr (such as ≤0.5). Somani et al. [23] proposed a model to predict the reversion type based on the chemical composition of the steel, adopting the Cr- and Ni-equivalents including some other elements in addition to Cr and Ni. Using this model, for instance, an AISI 301 reverses by the shear mechanisms above 670 °C, whereas a 301LN grade exhibits diffusion-driven transformation [23], controlled by the fast diffusion of interstitial nitrogen atoms [136]. This model has also been used by Misra et al. [88]. Shirdel et al. [70] adopted different equivalents including microalloy elements as predicting the reversion mechanism for a 304L steel. According to that prediction, the shear mechanism is possible above 783 °C. Based on microstructure features, the diffusion-controlled mechanism was the dominant one at the temperature range of 600–650 °C, and the shear reversion mechanism might be operative at temperatures higher than 750 °C. Sun et al. [137] reported diffusional reversion for a 304 ASS after a 85% cold rolling reduction and annealing at 550–650 °C at a low heating rate of 10 °C/s based on model predictions and observed

time-dependence of the reversion at 650 °C. However, Cios et al. [132] showed by the transmission Kikuchi diffraction measurements that the reverse transformation proceeded in a 304 ASS through a diffusionless mechanism.

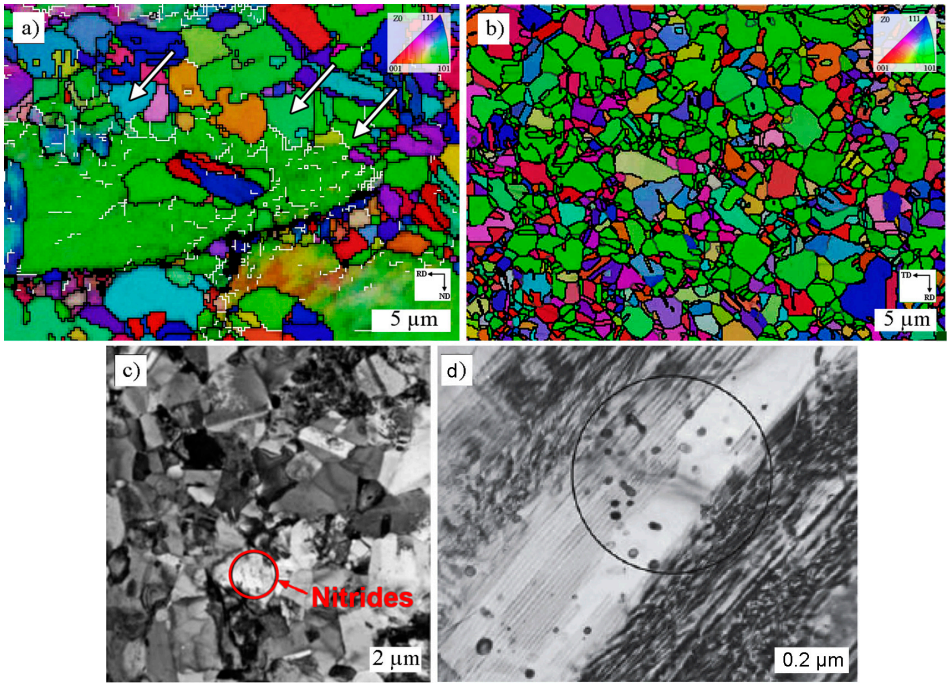

Figure 3. Reversion in 301LN ASS occurred by the shear reversion (**a**), where dislocation free grains are formed by continuous recrystallization (arrows pointing out such subgrains) [29], diffusional reversion (**b**) (reproduced from [84], with permission from Elsevier, 2017) and diffusional reversion with chromium nitride precipitation (**c**,**d**) (reproduced from [22], with permission from Springer Nature, 2007).

For a 301 ASS, microstructural observations of Johannsen et al. [135] indicated that it underwent a diffusional reversion from martensite to austenite in all annealed samples (90% cold rolled; heating rate 100 °C/min; annealed at 600–900 °C for 30 min) except when annealed at 800 °C and possibly at 850 °C while a shear reversion mechanism seemed to be active. Knutsson et al. [130] found that the diffusional reversion started at about 450 °C and the shear reversion at higher temperatures of 600 °C. In addition, carbo-nitride precipitation was observed for samples heat treated at these temperatures, which led to an increasing Ms-temperature and new α'-martensite formation upon cooling. They applied cold rolling reductions between 23% to 60%, but this did not affect the reversion rate.

Consistently with the above observations, Somani et al. [23] and Misra et al. [88] showed for a 301ASS that the shear transformation had occurred in the course of heating at a high rate of 200 °C/s or during annealing at temperatures around 800 and 900 °C. However, at 700 °C the reversion kinetics was clearly time dependent, i.e., the reversion was presumably diffusion controlled there (as mentioned above, the model developed predicted the start temperature of austenite formation As ≈ 670 °C for the shear transformation [23]). The continuous recrystallization of the shear-reversed austenite or the recrystallization of DA grains requires a higher temperature than the reversion itself does or it is slower than the martensitic reversion [121,138,139]. In a 301 grade, for the recrystallization that refines the GS following the shear reversion within few seconds, the temperature of 900 °C has been found feasible [23]. According to Sun et al. [140], in an 80% cold-rolled 304 ASS, the shear reversion took 1 min at 750 °C, while the recrystallization of DA grains required 15 min.

Yagodzinskyy et al. [134] investigated microstructural changes in 70% cold-rolled ASSs 301 and 301LN, containing 0.10% C and 0.16% N respectively, under slow linear heating at a rate of 15 °C/min and found the precipitation of carbides and nitrides respectively at martensite laths interfaces in the 301 steel and martensite/austenite interfaces in the 301LN steel. The start of reversion was at 550 and 500 °C

in these steels, respectively. In the 301, the reversion was diffusion controlled at 600 °C, but there was also 30% retained austenite after the cold rolling, and stripes of α′-martensite formed recurrently in the retained austenite by a mechanism which seemed to be shear. The bimodal grain structure with the 1 μm average GS was formed after recrystallization at 700–800 °C. In contrast, the new austenite grains grew continuously in the 301LN under diffusion control and a uniform GS of 0.35 μm was obtained.

On the other hand, the start A_s and finish A_f temperatures for the diffusional reversion depend on both the heating rate and chemical composition of the steel. The effect of heating rate was already investigated in Fe-Ni-C alloys by Apple and Kraus in 1972, who observed the shear mechanism at high heating rates and diffusional at low heating rates [141]. The diffusional reversion proceeds more rapidly with increasing annealing temperature, and the A_f temperature depends on soaking time. The transformation kinetics from martensite to austenite has been modelled in a 301LN ASS by Rajasekhara and Ferreira and found to be controlled by the diffusion of nitrogen [136]. Sun et al. [142] reported diffusional reversion for the 304 ASS (Ni/Cr = 0.49) after a 93% cold rolling reduction and annealing at 650–700 °C at a low heating rate of 10 °C/s. Tomimura et al. [39] found that the reversion was diffusional at 652 °C in an 18Cr-9Ni alloy (Ni/Cr = 0.5) in spite of a high heating rate of 300 °C/s.

Somani et al. [23,80], Kisko et al. [27,28,81–83] and Järvenpää et al. [84–87] have used a high heating rate of 200 °C/s in their experiments. They found that in 301LN (Ni/Cr ≈ 0.4), the diffusion-controlled reversion started, depending on prior cold rolling reduction, around 650–700 °C and was completed within few seconds at 750–800 °C. Examples of the influence of cold rolling degree on the reversion kinetics in a 301LN ASS are illustrated in Figure 4, where also the data of Takaki et al. [40] for an 18Cr-8.5Ni steel is included. A higher reduction results in faster reversion. The diffusional reversion is fast at 750 °C and above in both steels being completed within 100 s even after 45% cold rolling reduction.

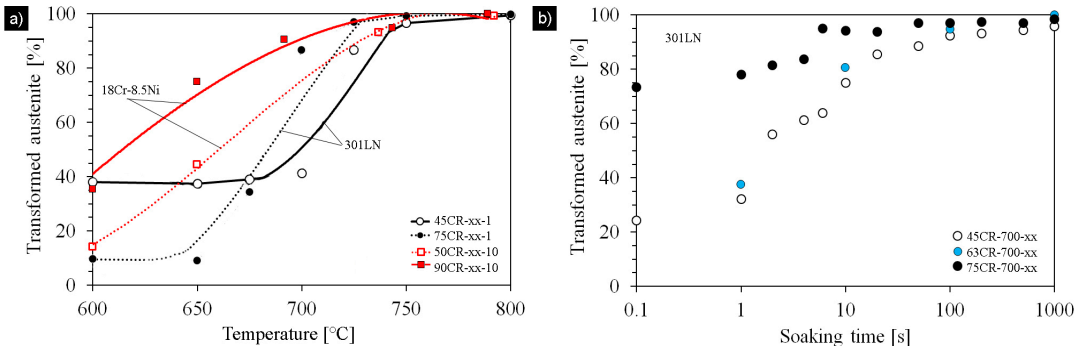

Figure 4. The effect of prior cold rolling reduction and annealing parameters on the reversion kinetics: Annealing temperature (**a**) and soaking time at 700 °C (**b**). Data collected from References [23,40] (**a**) and [23,26,88] (**b**). Legend: Reduction (%CR), annealing temperature (°C) and time (s).

However, under certain conditions, both the shear and diffusional reversion mechanisms seem to be active in a 301LN [84,102] and also in a 204Cu [82,101]. Guy et al. [35] found that in 18Cr-8Ni and 18Cr-12Ni ASSs the reverse transformation can proceed by both processes depending upon the heating time and temperature. Lee et al. [45] reported that in a 11Cr-9Ni-7Mn steel both mechanisms can occur sequentially, the diffusionless reverse transformation during continuous heating followed by the diffusive reverse transformation during the isothermal holding. Similarly, Knutsson et al. [130] pointed out that in a 301 ASS, the shear reversion only reverses 90% to 98% of the martensite, and a complete reversion can only be achieved by diffusional reversion for long holding times. According to Shakhova et al. [62], in S304H (18Cr-8Ni-2Cu-Nb) ASS after very severe caliber rolling to a total strain of 4, both reversion mechanisms were found to take place in annealing at 600–700 °C. The appearance of equiaxed austenite grains suggested diffusive reversion, while the elongated grains were signs of shear reversion. The latter was also indicated by the rather high dislocation density remained in the annealed microstructure.

3.2. Temperature Range for Reversion

The difference in the reversion mechanisms can be illustrated by the reversion-temperature-time diagram where the start and finish temperatures of the martensite reversion to austenite are drawn [39]. Moreover, from the diagram, it is possible to judge how the reversion process makes progress under certain conditions. In Figure 5, the respective temperatures are $A_{s'}$ and $A_{f'}$ for the shear reversion and A_s and A_f for the diffusional one. The martensitic shear reversion proceeds during heating in a narrow temperature range $A_{s'}$–$A_{f'}$. These temperatures depend on the chemical composition of steels being lowered by increasing the Ni/Cr ratio, but they are independent of the heating rate. The shear reversion rate is fast and independent of prior cold rolling reduction, and the reversed fraction is independent of isothermal holding time between these temperatures. The possible reversion treatment routes in Figure 5 are 1 and 2, leading to complete reversion, but the austenite grains can contain high dislocation density after short holding (route 1), or they can be dislocation-free and refined after sufficient holding (route 2).

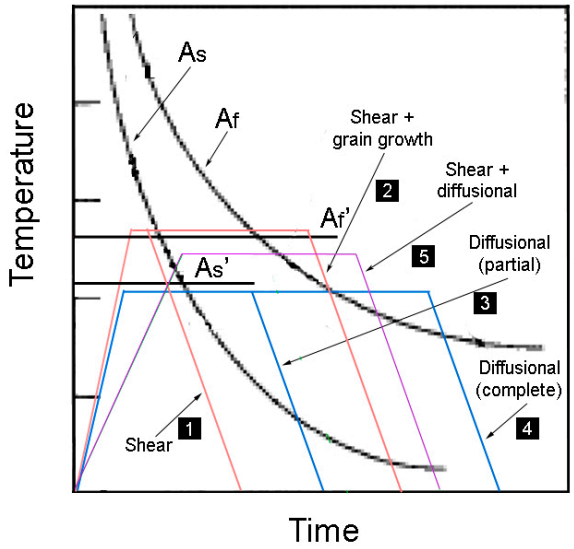

Figure 5. The temperature range for the reversion, dependent on the reversion mechanism. Various reversion treatments (numbered 1 . . . 5) are possible. The original idea of the reversion-temperature-time diagram is from Reference [39].

On the other hand, the A_s and A_f temperatures for the diffusional reversion depend on the heating rate in addition to the chemical composition of the steel (Figure 5). The effect of heating rate was already investigated in Fe-Ni-C alloys by Apple and Krauss [141] in 1972. In isothermal annealing, the diffusional reversion proceeds more rapidly with increasing annealing temperature, and the A_f temperature depends on soaking time, as seen from the A_s and A_f curves. The reversion annealing routes 3, 4 and 5 are possible, and a short holding (route 3) below $A_{s'}$ would result in partial reversion and a sufficiently long holding (route 4) to complete reversion. A slow heating to the $A_{s'}$–$A_{f'}$ regime means the initiation of shear reversion which might be completed by the diffusional reversion (route 5) or some DIM remains stable.

There are several studies where the reversion range of 304 ASS has been investigated, but quite different values for A_s (or $A_{s'}$) and A_f (or $A_{f'}$) have been reported. As mentioned above, the mechanism seems to change at around 750 °C from diffusional to shear type with increasing heating or annealing temperature. Guy et al. [36] reported A_s = 540 °C for an 18Cr-8Ni steel. Tomimura et al. [39] found by the saturation magnetization measurements a narrow reversion range 575–625 °C for a 90% cold-rolled 16Cr-10Ni steel where DIM reverted to austenite by the shear mechanism during heating at a high rate of 300 °C/s. Mumtaz et al. [143] estimated from the changes in the saturation magnetization for a 304 ASS (40% to 55% cold rolled, rapid heating, though the rate not given, 5 min holding) the A_s temperature

to be between 625–650 °C, and the A_f between 900–950 °C, hence a very wide range. At 700–800 °C, the reversion kinetics was dependent on the previous cold rolling reduction. Tavares et al. [144] obtained by thermomagnetic analysis the A_s and A_f temperatures during heating (heating rate was not given) as $A_s \approx$ 430–440 °C and $A_f \approx$ 610–616 °C. Cios et al. [63] determined A_s and A_f temperatures of 450 and 700 °C, respectively, from dilatometric curves. Shakhova et al. [62] data and ThermoCalc calculation for an Fe-0.1C-0.1N-18Cr-8Ni-2Cu-0.5Nb steel indicated the A_f temperature of 800 °C.

There are few studies on the reversion range itself in 301 and 301LN ASSs, although the reversion mechanisms have been investigated in numerous works. However, the A_f temperature for a 301LN ASS has not been clearly reported, and due to the diffusion-controlled reversion, it is dependent on cold rolling reduction and annealing duration, as evident from Figure 4. In that data, about 5%DIM is left after 10 s holding at 700 °C after the 75% reduction, while after the 63% reduction, Järvenpää et al. [84] reported 10% of DIM and Rajasekhara [26] 5% after 100 s and 20% after 10 s. Anyhow, in numerous studies, temperatures between 600 and 1000 °C have been used for reversion treatments of 301LN ASS [12,22–26,84–87].

For 201 and 201L grades, the temperature of 850 °C has been found to be an adequate reversion annealing temperature resulting in complete reversion within 30 s and in the finest GS [15,16]. Kisko et al. [27] obtained high tensile elongations (softened structure) in a 60% cold-rolled 201 ASS after 15 s at 800 °C. Sadeghpour et al. [69] found that in a 201L + 0.12Ti steel, the reversion rate depends on temperature and holding time, so that the reversion seemed to be diffusion controlled. The temperature of 900 °C was convenient for the reversion within a soaking time of 60 s.

4. Evolution of Reversion-Annealed Microstructures

In reversion annealing, a highly refined austenite GS is to be created. In this chapter the microstructure of reversion-treated ASS is discussed accounting for the fact that in practice the microstructure is not simple highly refined structure but is quite complex. Due to a limited cold-rolling reduction, the deformed structure consists of DA in addition to DIM, the latter deformed to various degrees. This results in non-homogeneous microstructure inherited from recrystallization of DA and reversion of DIM during the annealing stage. At low annealing temperatures, also recovered DA and retained DIM exist. In prolonged annealing, the grain growth of fine grains can be expected. The numerous studies to characterize and classify the microstructure are described with examples of GS and its distribution. Separately, a chance of repeating the reversion treatment or employing complex reversion routes have been mentioned, while looking for bimodal GS distributions.

4.1. Reversed Microstructures

The degree of cold rolling reduction prior the annealing influences on the reversed microstructure, e.g., [29,40,145]. After a high reduction, when the lath-martensitic structure is completely destroyed forming a cell structure, equiaxed austenite grains nucleate at random and grow in the recovered martensite matrix. In this case, small equiaxed austenite grains much below a micrometer can form during the full reversion. Instead, after a low cold rolling reduction, the DIM is still lath-martensitic, and reversed austenite nucleates on lath boundaries and forms a stratum structure of austenite laths and blocks. The reversed austenite just looks like a lath-martensitic structure. Guy et al. [36] found a twinned substructure in austenite. Finally, subboundaries in the shear-reversed austenite are gradually replaced in the continuous recrystallization process by high-angle grain boundaries forming thereby refined microstructure [29,38,40,54,146]. This happens especially after low cold rolling reductions [29].

However, if the microstructure contains both DIM and DA after cold rolling, different deformation states of DIM and DA tend to modify the microstructure, resulting in non-homogeneous GS distributions. In ASSs such as 304 and 316, grades where the austenite stability is high, low DIM fractions may be attained even after high cold rolling reductions (see Figure 2). Inhomogeneity in GS is a result of the reversion of DIM and the recrystallization of DA, the latter being often partial after low-temperature annealing. Similarly as in shear reversed austenite, the recrystallization of DA grains is sluggish in nature,

and it also seems to take place by a gradual evolution of subgrains and their subsequent transformation into fine grains, i.e., by the continuous recrystallization type process, e.g., [29,39,40,45,54].

Järvenpää et al. [29,84] have investigated in detail the reversed microstructures created at low annealing temperatures after low cold rolling reductions and pointed out the complexity of the microstructure, consisting of fine-grained reversed austenite, DA with different recrystallization degree and retained DIM. They showed in reversed structures obtained at low temperatures (<800 °C), in addition to micron-scale reversed grains and coarse DA grains, the presence of medium-sized (GS range 3–10 μm) grains. Medium-size grains are formed from slightly deformed DIM so that their fraction depends on rolling reduction and annealing temperature. In Figure 6, examples of different microstructures created in a 301LN are displayed revealing a broad variation of the reversed austenite GS. In addition to the annealing temperature, the cold rolling reduction has a significant influence, whereas the fraction of slightly deformed austenite increases with decreasing rolling reduction [29,102].

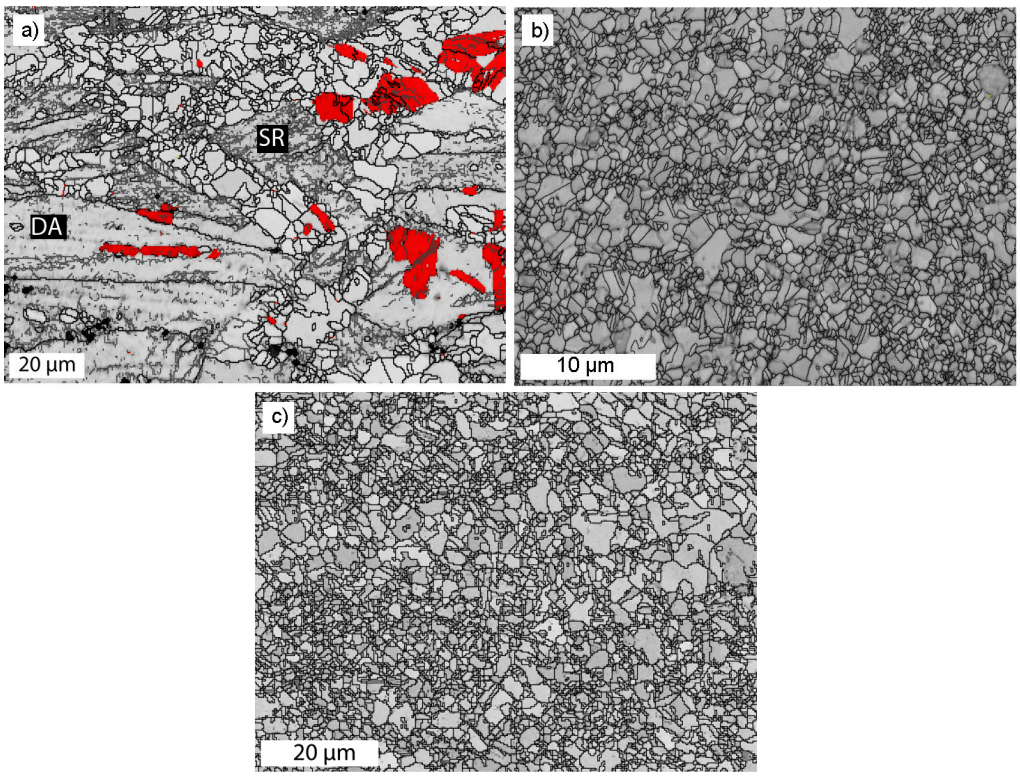

Figure 6. Examples of reversed microstructures in 301LN with various grain size. Partially reversed (32% cold rolling, 750 °C for 0.1 s) with shear reversed (SR) fine and medium-size grains, a large DA grain and retained DIM (red colored phase) (**a**) and diffusionally reversed ultrafine and medium-size grains in 63% cold-rolled steel, annealed at 800 °C for 1 s (**b**) and at 900 °C for 1 s (**c**).

A further factor resulting in non-homogeneous GS distribution is the elemental segregation present even in cold-rolled and annealed ASS sheets. Man et al. [100] have pointed out that the 301LN grade exhibits pronounced manganese banding, which is experienced in differences in the stability of austenite during cold rolling and consequently in GS after reversion annealing.

However, heterogeneous GS has been found to be beneficial especially for the ductility of ASSs (see more in Section 5), and therefore, in numerous studies, special processing routes have been applied intentionally to create such a structure. Ravi Kumar et al. [146] reported GS distribution varying widely between 100 nm and 2 μm after two-stage annealing of a 90% cold-rolled 316L ASS, resulting in a good combination of YS and ductility as compared to the coarse-grained counterpart after annealing at temperatures above 900 °C. Sun et al. [146] applied three cold rolling and annealing stages for a 304 ASS to obtain a GS of 150 nm providing good mechanical properties. In a more recent study,

Sun et al. [140] reported that in two-stage annealing of a 304 ASS containing 47% DIM and 53% DA after two-stage cold rolling (67% + 47%, respectively) at 800 and 850 °C, non-uniform grain structure was created, where the fraction of ultrafine grains (<1 μm) decreased and larger austenite grains (up to 3 μm) increased with prolonged annealing. Ravi Kumar et al. [18,146,147] and Ravi Kumar and Raabe [148] have obtained bulk ultrafine-grained ASS with mono- (maximum at GS ≈ 0.6 μm) and bimodal-type (minimum at GS ≈ 0.5 μm and maximum at GS ≈ 1.40–1.65 μm) GS distributions by 4-stage cyclic thermal processing in a 90% cold-rolled AISI 304L grade. This enhanced significantly the elongation. Roy et al. [117] also reported a bimodal GS distribution in a cryo-rolled 304L grade after annealing at 700–800 °C. The GS was very fine: one group between 50–100 nm and the other 200–300 nm from DA. A beneficial contribution to ductility was claimed. Poulon-Quintin et al. [30] obtained a bimodal grain structure consisting of ultrafine-grained austenite with average GS equal to 0.5 μm as a consequence of martensite reversion together with bands composed of recrystallized fine grains of 2.0 μm from strain-hardened austenitic bands in a 15Cr-9Ni-3Mo steel, which was 80% cold rolled forming 75%DIM and 25%DA.

In principle, the grain growth tendency of reversed very fine grains is high during the initial period of annealing (1–100 s) due to the high curvature of grain boundaries and consequently large driving forces for grain growth [26,89]. The value of the activation energy of grain growth was found by Rajasekhara et al. [26] to be equal to that of conventional ASSs (~205 kJ/mol). Kisko et al. [82] obtained much higher values for a Nb-microalloyed 204Cu grade, the value increasing from 363 to 458 kJ/mol with the increasing Nb content. Some experimental results for the growth of reversed fine grains in 201L, 204Cu, 301LN and 304 ASSs have been collected in Figure 7, revealing the trends at 800 and 900 °C. There is some difference between the data of 304L [17,70] and 304 [11] at 900 °C, but the processing of the structures was also different. Anyhow most importantly, the data indicate that grains do not grow much at 800 °C, if a GS of around 1 μm is concerned. The grain growth can also be retarded effectively by microalloying. The influence of Nb [19,82,83,101] and Ti [68] microalloying for restricting the grain growth has been determined. For instance, the grain growth was effectively retarded in a 204Cu ASS by 0.28 wt. % Nb alloying even at 1100 °C and by 0.11 wt. % Nb at 1000 °C [82].

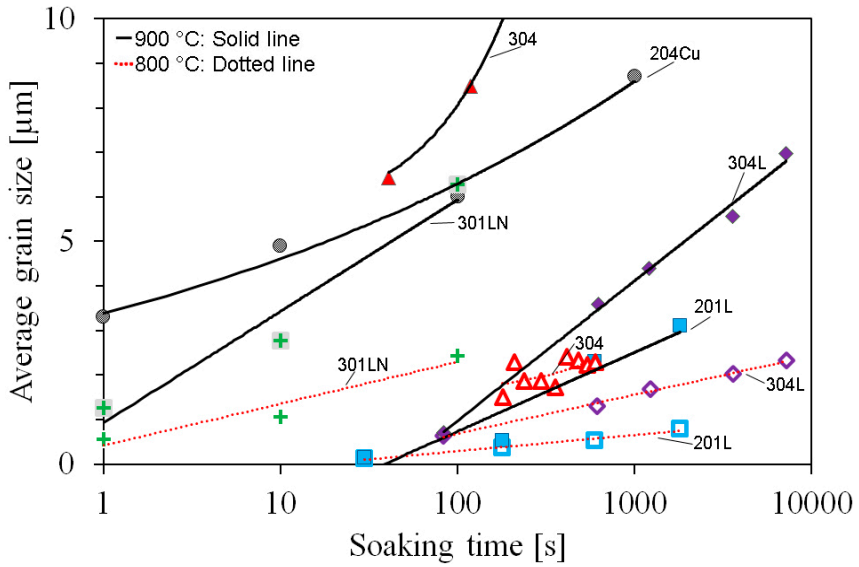

Figure 7. Grain growth of reversed grain size at 800 and 900 °C in 201L [67], 204Cu [82], 301LN [26], 304L [17,70] and 304 [11] ASSs.

Table 2. Examples of grain sizes and mechanical properties achieved in reversion treatments of Cr-Mn, Cr-Ni and some special austenitic stainless steels.

Grade	CR	T	t	GS	YS	TS	TE	Ref.	Grade	CR	T	t	GS	YS	TS	TE	Ref.
	[%]	[°C]	[s]	[µm]	[MPa]	[MPa]	[%]			[%]	[°C]	[s]	[µm]	[MPa]	[MPa]	[%]	
201	90	850	30	0.1	1370			[15]	301LN	80	700	1200	0.76	830	953	36	[47]
	60	800	2		770	1155	27	[28]		77	800	1	0.6	880		44	[91]
			15		686	1020	31	[28]		76	800	1		768	1060	43	[23]
			40		629	964	37	[28]			700	10		1004	1106	38	[23]
201L	95	850	30	0.07	1485	1780	33	[16]		63	800	1	0.54	720	1060	35	[22]
			180	0.14	1075	1710	37	[16]		60	800	1		711	995	50	[23]
		800	30	0.06	1300		33	[67]			700	100		901	1106	37	[23]
			180	0.35	1070		24	[67]		56	790	80	0.9	670	1030	55	[87]
201L-0.23N	60	800	1	0.5	1100	1260	30	[80]			690	60	0.7	815	1105	45	[87]
			10	1.5	800	1100	50	[80]			680	45	0.7	855	1135	44	[87]
			100		680	1020	58	[80]			660	30		985	1160	29	[87]
201-0.3Nb	90	900	60	0.09	1000	1500	35	[71]		50	800	160		798	1057	38	[12]
201Ti	90	900	60	0.05	1000	1330	42	[69]				107		773	1023	41	[12]
		850	60	0.05	1005		36	[68]				80		645	1036	41	[12]
		750	600	0.13	856		34	[68]			750	160		778	1057	32	[12]
204Cu	60	800	1		723	1041	47	[28]				107		682	1063	35	[12]
			1		606	1093	45	[83]				80		709	1042	35	[12]
		700	10		1185	1308	43	[83]		45	800	160		682	1000	46	[12]
			100		899	1345	37	[83]				107		662	1017	39	[12]
			1000		605	1180	36	[83]				80		644	1017	46	[12]

Table 2. *Cont.*

Grade	CR [%]	T [°C]	t [s]	GS [µm]	YS [MPa]	TS [MPa]	TE [%]	Ref.	Grade	CR [%]	T [°C]	t [s]	GS [µm]	YS [MPa]	TS [MPa]	TE [%]	Ref.
204Cu-0.45Nb	60	800	1		997	1187	51	[83]			750	160		809	1125	37	[12]
		700	10		1141	1297	40	[83]				107		785	1089	35	[12]
			100		1124	1319	40	[83]				80		748	1068		[12]
			1000		1015	1258	31	[83]			760	85	1.1	590	1030	57	[87]
301	95	850	1	0.07	1970			[65]			695	65	0.8	750	1080	54	[87]
	60	850	10		609	1122	36	[28]			675	45		780	1100	50	[87]
		750	10		1001	1318	28	[28]		32	820	130	1.6	520	1000	62	[87]
	52	900	1		584	1032	44	[23]			690	70	1.2	785	1140	51	[87]
		800	1		1070	1290	28	[23]			660	40		915	1135	32	[87]
			10	0.5	1000	1250	35	[88]		20	750	600	2.9	749	1010	33	[60]
304	90	750	1200	1.02	550	840	41	[11]		0			20	331	815	62	[12]
	85	580	1800	0.15	1120	1440	12	[137]						350	831	62	[12]
	80	700	60	0.15	1020	1160	8	[50]	304L	90	900	120	2.2	994	1160	40	[20]
	70	750	600	1 / 0.2	950	1050	47	[148]			700	1200	0.14	1000	1010	40	[14]
												18000	0.33	1000	1010	40	[14]
17.1Cr-11.3Mn-0.27N	85	850	100	0.85	900	1100	60	[72]		65	850	60	0.62	885	1385	44	[70]
		750	10	0.5	1450	1500	19	[72]		67	550	150	0.27	1890	2050	6	[48]
17Cr-6Ni-2Cu	75	700-900		0.22	980	1100	30	[51]		67	650	180	0.8	1170	1350	12	[48]
										0			35	220	1640	59	[48]

CR, Cold rolling reduction; T, annealing temperature; t, holding time; GS, grain size; YS, proof/yield stress; TS, tensile strength; TE, total elongation.

4.2. Repeated Reversion Treatments

Commonly, the prior austenite GS has an influence on its decomposed structure. Does the original GS affect the reversed structure? As a reversion treatment refines the GS, it is expected that by repeating the reversion treatment further refinement can be achieved. Ma et al. [21] repeated the conventional reversion treatment twice (75% reduction, annealing at 650 °C for 10 min + 50% reduction and annealing at 630 °C for 10 min) in an Fe-0.1C-10Cr-5Ni-8Mn alloy. After the first reversion, the structure consisted of nearly equiaxed austenite grains with the average size of about 300 nm, whereas after the second reversion, some grains are even smaller than 100 nm while others are a little larger than 200 nm. The YS increased from 708 MPa to 779 MPa by repeating the reversion, but the elongation decreased from 36% to 32%.

As mentioned in the previous section, in order to create the bimodal GS distribution, special reversion treatments with several rolling and annealing stages have been executed in processing of 304L steel. Sun et al. [137] have used three-stage processing and also two reversion stages [140]. Ravi Kumar et al. [147] and Ravi Kumar and Raabe [148] have employed complex rolling and annealing schedules, with iterative and isothermal annealing periods. The present authors have also applied various repeated schedules to 301LN ASS and obtained further GS refinement and higher uniformity of the grain structure. However, concerning industrial purposes complex reversion annealing treatments are hardly very interesting or practical, although a treatment repeated twice has been utilized [104,107].

5. Properties of the Reversion-Treated Structures

For steel users, the mechanical properties are important, and the reversion treatment is intended to enhance them, especially the YS of ASSs. In this extensive chapter, the tensile properties will first be discussed based on the vast experimental data collected from the literature, mainly for reversion-treated commercial Cr-Mn and Cr-Ni ASSs. The influence of the GS on YS has been analyzed. The enhanced YS-ductility combinations achieved are highlighted as a practical result while employing the reversion process. Further, the excellent tensile ductility being affected by the stability of the austenite has been discussed in detail. The effect of highly refined GS on the stability, a somewhat disputed issue, will be considered. Particularly, the influence of carbide/nitride precipitation occurring in many ASSs during reversion annealing reducing the stability, but neglected in many studies, will be addressed. The deformation mechanisms and the related strain hardening rate are also discussed, which is interesting in trying to understand the background of high ductility.

In a separate section, fatigue properties will be described showing distinct advantages attained from the reversion treatment if based on fatigue resistance under a given stress amplitude. Finally, the other properties, though more rarely investigated, such as the formability, weldability, corrosion resistance and surface properties for medical applications, will be considered, highlighting that they are comparable or better than the corresponding properties of conventional coarse-grained ASSs.

5.1. Tensile Strength Properties

A principal target of the reversion treatment is to increase YS of an ASS without impairing its high elongation. An example of typical results is illustrated in Figure 8, where a set of engineering stress–strain curves are plotted for a 301LN ASS showing how significantly YS is increased by refined GS as a result of reversion treatments. Moreover, the tensile strength (TS) is improved while TE is decreased. Certain typical changes, a yield point and a concave shape, appear in the flow curves, to be discussed later.

In order to give a view of the current state, some data concerning the mechanical properties of reversion treated ASSs were collected from the literature and listed in Table 2. In addition, the cold rolling reduction, annealing temperature and duration as well as the (average) GS are given in the list if available. The commercial steel grades 201/201L, 301/301LN and 304/304L mostly investigated are

included. Some data are also for a 204Cu and Ti- or Nb-microalloyed 201and Nb-microalloyed 204Cu as well as for a couple of austenitic alloys.

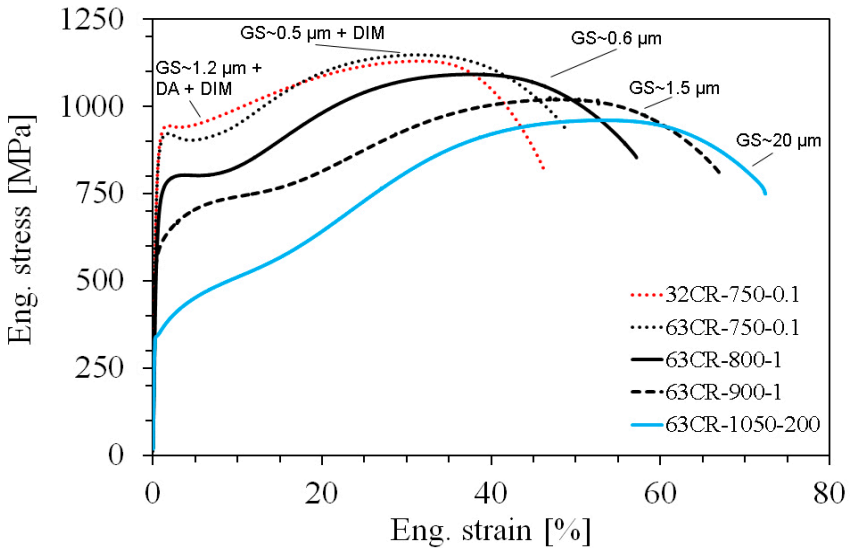

Figure 8. Examples of engineering tensile stress–strain curves for a 301LN ASS with refined grain size after various reversion treatments. Data collected from References [87,102,103]. Legend: Reduction (%CR), temperature (°C), duration (s).

From the data in Table 2, a general conclusion can be drawn that no distinct difference exists between the Cr-Ni and Cr-Mn type grades, and same temperatures between 650–900 °C and holding times 1–1800 s are feasible for the reversion. It seems that the YS (proof stress, $R_{p0.2}$) values reported for 201/201L ASSs can be well above 1000 MPa, even up to 1485 MPa [16], but in those instances severe cold rolling reductions of 90% to 95% have been applied to obtain the GS of an order of 60–100 nm. However, the 60% cold rolling of 201 with 0.23%N [80] similarly as 204Cu and 204Cu-0.45Nb [83] can result in YS of 1.1 GPa, while TE is still about 40%.

YS values of the reversion-treated 301/301LN ASSs achieved are typically over 700 MPa and up to 1 GPa, i.e., 2–3 times compared to the YS of respective commercial annealed sheets. Further, the reversed structures obtained at low temperatures (800 °C and below) exhibit significantly enhanced YS compared to the structures created at temperatures of 900 °C. Then, a slight upper yield point appears with discontinuous yielding (Lüders strain), as seen in Figure 8 [87,103].

Moreover, the 304 and 304L grades require a high cold rolling reduction at lowered temperatures, as pointed out in Section 2 (Figure 2), and then, comparable strength values have been obtained. It can be noted that exceptionally high strength values have been reported by Shen et al. [48] for a 304L ASS after 67% multipass warm rolled at 400 °C, which formed 73% of DIM. After annealing at 550 °C for 150 s, the reversed GS was 0.27 µm and the amount of retained DIM 32%. As listed in Table 2, the tensile properties reported were extremely high, YS 1890 MPa, TS 2050 MPa and TE 6%. Moreover, annealing at 650 °C resulted in high strength. YS values around 2 GPa with reasonable ductility have also been reported by Rasouli et al. [72] in interstitially alloyed Ni-free Cr-Mn grain-refined ASSs with a low C/N ratio. It can be mentioned that very recently, Xu et al. [149] have shown that the refined GS in an 18Cr-8.3Ni ASS exhibits the enhanced YS and YS-ductility combination in relation to its coarse-grained counterpart also at elevated temperatures, up to 600 °C.

Concerning the influence of the degree of cold rolling on YS, Somani et al. [23] and Misra et al. [24] reported that the YS of completely reversed structure in a 301LN steel, created at 800 °C–1s, increased from 800 to 950 MPa with increasing the reduction from 45% to 77%, while the TE remained practically unchanged (about 43%). This can be understood as a result from GS refinement due to the heavier cold rolling. However, the prior cold rolling reduction in the range of 32% to 63% did not affect

markedly the mechanical properties of the low-temperature partially reversed structures, where a larger, non-uniform GS will be balanced by stronger retained phases, DIM and DA [87]. Experiments using induction heating indicate that the annealing temperature (660–820 °C) has an essential influence on YS, for it increased with decreasing the peak temperature, but any influence of the cold rolling reduction between 32% and 56% has not been realized (see Table 2) [87]. Regarding the YS of 201/201L ASS, it seems that the cold rolling reduction of 50% to 70% has resulted in considerably lower values (YS ≈ 400–750 MPa) than the reduction of 90% to 95% has done (YS above 1000 MPa), although the data are quite scarce. For instance, Rasouli et al. [72] have reported high YS values for a 17Cr-11Mn-0.275N ASS, YS 1450 MPa and TE 19%, although the 80% cold rolled structure contained 53% DIM only.

The evident fact is that the TS cannot be increased so significantly as the YS, only about 200 MPa to reach the level of 1100 MPa in most cases. This is due to somewhat lower strain hardening rate (SHR) owing to finer GS generally increasing the austenite stability and shorter elongation in reversed fine-grained structures (Figure 8).

The background mechanisms of high YS of reversion treated ASSs have been analyzed in some papers. For instance, in completely reversed structures of 301LN, the strengthening contributions of solid solution, precipitation, dislocations and GS have been evaluated, the values being approximately 200, 120, 40, 250 MPa respectively (annealing at 800 °C for 1–10 s; GS ≈ 0.54–1 μm) [22]. Thus, refined GS is an important strengthening factor. Moreover, Kisko et al. [83] estimated the amount of GS strengthening to be about 300 MPa in a 204Cu ASS as annealed at 900 °C for 10 s (GS 1.4–1.9 μm).

The Hall–Petch relation between YS and GS has been reported in numerous studies. Di Schino et al. [10] found that it holds down to 3 μm GS for a 301 ASS, and according to Huang et al. [47] at least down to 0.74 μm GS for 301LN and even to 0.135 μm GS for a 304L according to Forouzan et al. [14]. In structures reversed at low temperatures, the amount of precipitation in certain grades, the retained phases and their annealing state are additional contributors, so that it is obvious that any exact relationship between GS and YS cannot be expected for them. The several features affecting the Hall–Petch relationship for YS vs GS of reversed structures were discussed by Rajasekhara et al. [22]. Anyhow, several relationships have been proposed, and some examples are shown in Figure 9. Shakhova et al. [62] reported the slope 395 $\mu m^{-0.5}$ and the friction stress σ_o = 205 MPa for the data collected for Cr-Ni ASSs from the literature. Kisko [101] analyzed the literature data for Cr-Ni and Cr-Mn steels and realized a wide scatter, the slope varying in the range 256–377 $\mu m^{-0.5}$ and the σ_o between 241–428 MPa. Moreover, Järvenpää [102] has found a marked scatter especially in the slope, being in the range 261–576 $\mu m^{-0.5}$, while σ_o is 225–273 MPa. The GS is not uniform in many instances in the reversed structure, which is an apparent reason for the scatter in the values of the coefficients in the Hall–Petch relationship. A modified Hall–Petch relation has been suggested to account for the grain size distribution [150] but not applied to reversed structures.

As mentioned, Shen et al. [48] reported very high strength values close to 2 GPa for a 304L with very fine GS. Both DIM and mechanical twins were found to be effectively suppressed during tensile testing due to the refinement of GS so that the background of the strength seemed to be mainly the strengthening due to GS refinement. However, from the Hall–Petch relationship in Figure 9, it is expected that the GS of 270 nm (corresponding to 1.92 $\mu m^{-0.5}$) would result in YS of 1000 MPa, not close to 2 GPa. It can be concluded from the microstructural data that the structure annealed at 550 °C consisted of 41% reversed austenite (supposed to be formed by the diffusional mechanism), 32% retained recovered martensite and 27% DA. Therefore, it remains unclear, how the complex microstructure behaved to result in the GS of 270 nm and why this microstructure and GS provided the YS as high as 1.89 GPa. The dislocation structure must have a prominent contribution. As mentioned, the temper-rolled cold strengthened ASSs show directional anisotropy, so that the YS is lower in parallel than in transverse direction to the rolling direction [3,4]. However, the experiments have shown that this anisotropy disappears in completely reversed structure suggesting that it is related to the deformation in austenite [28,101]. This means that the reversed structure without any directional anisotropy can have the YS of about 650 MPa.

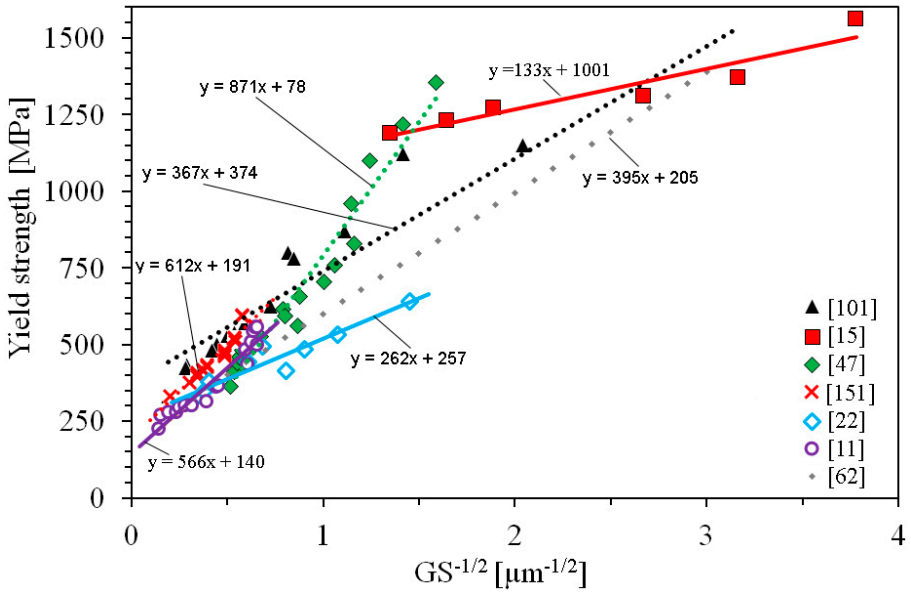

Figure 9. Examples of the Hall–Petch relations presented for reversed structures. Data for annealed coarse-grained 301LN is included from [151].

5.2. Tensile Ductility and Austenite Stability

5.2.1. Tensile Elongation

It is notable that the elongation values of reversed ASS structures are good in spite of high strength, though slightly decreasing with increasing YS, as seen in Figure 8. Generally, the TE is in the range of 30% to 40% even for the structures with the YS ≈ 1 GPa. It should, however, be noticed that many reported elongation values have been measured using non-standard tensile specimens with a short gauge length (15–25 mm instead of 80 mm), which may give too optimistic values.

In order to highlight the excellent strength-ductility combinations achieved with reversion-treated ASSs, YS vs TE combinations for 2XX and 3XX series, steels listed in Table 2 are plotted in Figure 10 together with some technical data for commercial temper-rolled steels and a trend line for the latter. The data though scattered indicate that many of the combinations achieved by reversion treatments are better than those obtained by temper-rolling. The combinations for 201/201L seem to distribute in two groups, well above the trend line and slightly below that, whereas for 301LN, they form one group above the trend line of the temper-rolled steels. From Table 2, it is seen that the higher values of 201/201L are obtained when very high cold rolling reductions are employed in the reversion treatment, whereas lower reductions are not so effective in GS refinement and increasing strength.

Furthermore, it has been found that the directional anisotropy, present in temper-rolled steels, is absent in completely reversed structures without DIM and DA [28]. The anisotropy appears in cold rolling of 5% reduction so that the texture cannot be the reason for that, but the dislocation structure. This means in practice that a steel with its YS order of 700 MPa can be manufactured without the directional anisotropy. Strength values in compression are not available so that they cannot be compared with tensile properties.

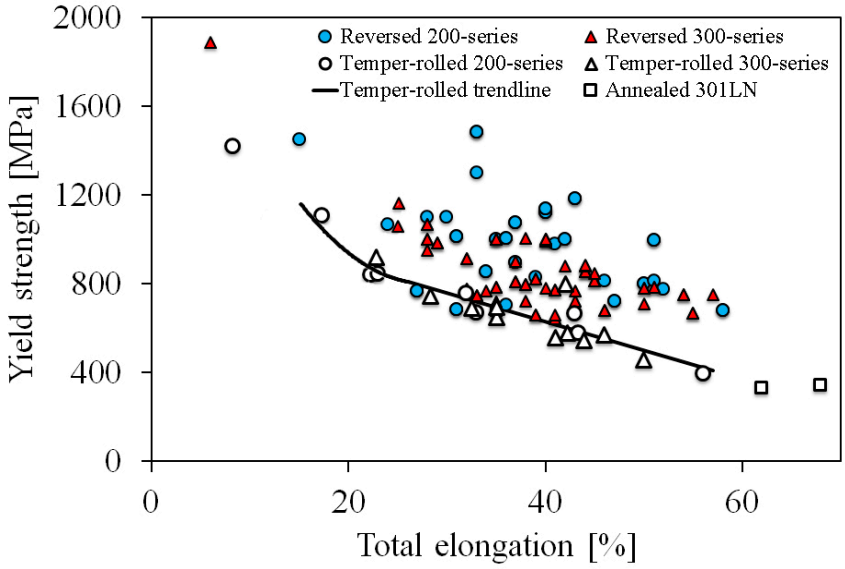

Figure 10. Yield strength-total elongation combinations for some reversion-treated steels listed in Table 2 compared to those of annealed 301LN and temper-rolled 301LN and 201L steel.

5.2.2. Elongation and Austenite Stability

In principle, the stability of austenite while transforming to martensite affects the strain hardening rate (SHR) and may influence on the ductility via the TRIP effect [152]. According to scarce data of Guo et al. [153], the tensile elongation of 301 ASS (M_{d30} = 39 °C) increases about 5%-units with increasing DIM fraction formed at different test temperatures, although the effect is quite marginal compared to the influence of martensite on SHR and TS. Cios et al. [63] measured the maximum elongation in a 304 ASS at −10 °C where about 50%DIM was formed. However, tensile tests at different temperatures by Weiss et al. [154] showed that the maximum uniform elongation for a 304L ASS is obtained at test temperatures of 20–40 °C, where only few per cents of DIM had formed, whereas the elongation decreased while more DIM was formed at lower test temperatures. They also refer to 11 investigations, which indicate that the maximum uniform elongation is obtained in conditions when about 20% of DIM was present. Talonen [155] also found that the elongation is highest at test temperatures where only a relatively low amount of DIM was formed in 304 and 301LN ASSs. In agreement, Hamada et al. [156] measured the maximum elongation at 50 °C for 201 and 201L ASSs, showing only 0% to 20% of DIM.

The rate of DIM formation in ASSs is classically described by the sigmoidal equation (OC-model) developed by Olson and Cohen [157]. The OC-model assumes that shear band intersections act as nuclei for martensite and that the nucleation and growth process of α′-martensite can be described by two parameters, α and β, as in the following equation:

$$f_{\alpha'} = 1 - exp\left[-\beta(1 - exp[-\alpha\varepsilon])^m\right] \quad (3)$$

where $f_{\alpha'}$ is the martensite fraction, ε is the true strain, α and β are parameters and m is the fixed exponent. The parameter α describes the rate of the shear band formation, assumed to be mainly dependent on the stacking fault energy (SFE) and strain rate. The parameter β is proportional to the probability that the α′-martensite is nucleated at a shear band intersection, being dependent on the chemical driving force and temperature. The exponent m describes the rate of the formation of the shear band intersections, often found to have the constant value of 4.5. In cold rolling, Forouzan et al. [14] reported α = 3.041 and β = 3.786 for AISI 304L (M_{d30} = 12.9 °C) and Somani et al. [23] α = 2.2 and β = 4.4 for 301LN (M_{d30} = 26.6 °C). The existing models used to predict the increase in the volume fraction of martensite with strain were examined and modified by Lichtenfeld et al. [158] to fit the

experimental data for a metastable 304L and stable 309 ASSs as well as data for 304 and 301LN collected from the literature. They reported values $\alpha = 3.0$ and $\beta = 4.3$ for 304L ($M_{d30} = 2$ °C) and $\alpha = 5.65$ and $\beta = 4.03$ for 301LN ($M_{d30} = 37$ °C) in tensile tests at a low strain rate avoiding adiabatic heating. Talonen [155] observed that the OC-model fitted well with his tensile test data, obtained at low strain rates, with $\alpha \approx 11.7$ and $\beta \approx 6.1$ for a 301LN steel ($M_{d30} \approx 23$°C). A recent logistic model was mentioned in Section 2, presented for 304 ASS cold-rolled to different reductions [124]. In that paper, also the limitations of the OC-model have been discussed.

In ultrafine-grained austenite, no shear bands are formed, but martensite nucleates on grain boundaries [75,81,102], so that the basis of the OC-model could be doubted. However, sigmodal shapes of DIM fraction vs strain have still been recorded (as seen in Figure 11). Marechal [75] even fitted his tensile data with the OC-model and determined the values of the parameters and their GS dependence, down to 0.5 µm GS. However, it is hard to draw any conclusions from the varying values of all the parameters.

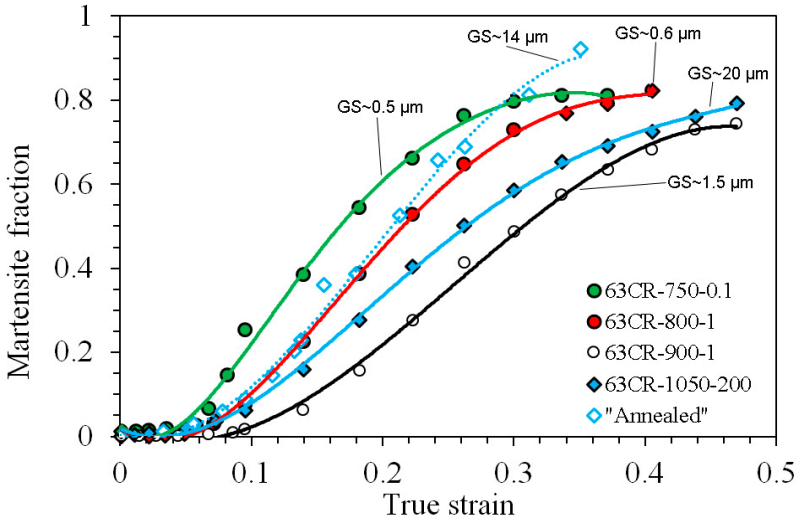

Figure 11. Examples of DIM evolution during tensile testing in various 301LN ($M_{d30} = 27$ °C) structures [82,85,87] and coarse-grained annealed 301LN with $M_{d30} = 37$ °C from Reference [155]. Legend: Reduction (%CR), temperature (°C), duration (s).

The austenite stability also depends on GS, as indicated by the Nohara equation (Equation (1)) for coarse grain sizes. Yoo et al. [159] found that DIM fraction after tensile fracture decreased from 60% to 25% with decreasing GS from 2 µm to 0.3 µm in a 10.30Cr–8.14Ni-7.47Mn steel. However, Matsuoka et al. [160] reported that the mechanical stability does not depend on GS in ASSs, because the martensite transformation is not necessarily multi-variant under tensile strain/stress, but the single-variant martensitic transformation is favored.

Marechal [75] and Järvenpää et al. [84] have extensively studied the stability of austenite in tensile testing in various reversed grain-refined structures of 301LN ASSs. Figure 11 shows examples of DIM vs strain in tensile tests determined by the latter authors. Generally, refining the GS down to about 1 µm was found to increase the stability, similarly to the GS change from 20 to 1.5 µm in the figure, but surprisingly, submicron-sized austenite was more unstable (GS of 0.6 and 0.5 µm) than the coarse-grained austenite [84]. Similarly, Kisko et al. [81] noticed the same trend in a 204Cu steel. Marechal [75] and Kisko et al. [81] explained the reduced stability of submicron grains by DIM nucleation on grain boundaries as a single variant (block), whereas the nucleation occurred at shear band intersections in the coarse-grained structure. Ravi Kumar and Gujral [161] and also Lee et al. [162] have reported DIM nucleation at the vicinity of grain boundaries in ultrafine-grained ASSs, although this was not related to a lower stability in their studies.

However, according to Järvenpää et al. [86], the real reason of the lower stability appearing in certain grain-refined structures in the 301LN ASS is the precipitation of chromium nitrides while annealed at low temperatures such as 650–800 °C (the curves for GS of 0.6 and 0.5 μm obtained at 800 and 750 °C, respectively, shown in Figure 11). A similar drop in the stability was observed by He et al. [163] in the low-temperature (800 °C–30 min) reversed structure of 321 (17Cr-8Ni-0.3Ti) ASS as comparing with the structure formed at 1000 °C. The reason for the low stability was suggested to be carbide precipitation. In consistence, Saenarjhan et al. [164] and Kim et al. [165] have reported the decrease of the austenite stability in a 15Cr-15Mn-4Ni steel due to $M_{23}C_6$ carbide precipitation during long-term annealing of the austenitic structure at around 800 °C. Johannsen et al. [135] noticed in a 90% cold-rolled 301 ASS, while annealing temperatures above 750 °C, an increase in the amount of martensite, which was formed during cooling. $(Fe,Cr,Mo)_{23}C_6$ carbides were formed within the grains and at grain boundaries, being an obvious reason for the reduced thermal stability of the reversed austenite. Moreover, Karimi et al. [166] observed new martensite forming during cooling in a 301 ASS, containing 0.11%C, after annealing at 900 °C for 100 min due to carbide precipitation.

Moreover, the results of Kisko et al. [83] reveal increasing DIM fraction after tensile testing of a 204Cu ASS while annealed at 700 °C for 1000 s, and the carbide or/and nitride precipitation could be the reason for that, though not confirmed. Lei et al. [51] found lower stability of a nano-ultrafine-grained (220 nm) structure of a 0.06C-17Cr-6Ni-2Cu steel compared to that of the coarse-grained (25 μm) structure, but they did not present any explanation. Huang et al. [47] have reported much lower stability of a ultrafine-grained 301 steel (GS 270 nm, deformed by ECAP and annealed for 1 h at 580–620 °C resulting in reversion) compared to a coarse-grained (GS 84 μm) counterpart during tensile straining. They suggested that micro-twins present in ultrafine grains could act as potential nucleation sites for martensitic transformation grains. However, the carbide precipitation might be the potential reason.

The annealing durations in most of the above-mentioned studies were quite long, 0.5–1 h. According to Kim et al. [165] the precipitation of carbides and Cr_2N in annealed austenite (Fe-0.2C-15Cr-15Mn-5Ni-0.2N) seems to be quite a slow process even at 700–800 °C. However, Järvenpää et al. [86] predicted that Cr_2N can start to precipitate in fine-grained austenite in a 301LN ASS within 10 s at 750 °C, and 0.15%N could be precipitated in 100 s. Evidently the precipitation can be very fast during the reversion treatment. Rajasekhara et al. [22,26] found by TEM nano-size CrxN precipitation within 1 s at 700–800 °C during reversion annealing. The precipitation took place presumably already in deformed martensite, where it is much faster than in annealed austenite. Hong et al. [167] observed that 30% tensile prestrain intensified precipitation in 347 type ASS, where carbides were formed in annealing at 650 °C around deformation bands. Knutssen et al. [130] found carbo-nitride precipitation in samples heat treated at 750 and 800 °C for 1 h after 61% cold rolling, but not after 23% reduction, indicating that high deformation was essential having the influence on diffusion rate and the rate of precipitation.

In 301LN ASS, the nitrogen is the element precipitating during reversion annealing. Lee et al. [162] reported only insignificant promoting effect of the depletion of solute atoms near high Cr-bearing particles of 10 nm in size and 3 nm Nb-bearing particles in a 70% cold-rolled Fe-0.1C-10Cr-5Ni-7.7Mn-0.3Nb steel, annealed at 664 °C for 10 min, on the total DIM fraction in tensile testing. However, Saenarjhan et al. [164] showed that the stability of austenite against martensitic transformation is enhanced with increasing C or N content, and N is a more effective element at an equivalent concentration. It is possible to estimate the potential effect of nitrogen precipitation in a 301LN ASS, considering the difference in the DIM formation between the data of Talonen et al. [155] in a 301LN with the M_{d30} = 37 °C and data reported by Järvenpää et al. [84,85,87,102] and Somani et al. [23] for another 301LN with the M_{d30} = 27 °C. These DIM vs strain curves are "Annealed" 14 μm GS and "63Cr-1050-200" 20 μm GS in Figure 11. For instance, at 0.2 true strain, the DIM fractions are about 45% and 32% in these steels, respectively. Thus, the difference of 10 °C in M_{d30} seems to result approximately in a 13% difference in the DIM fraction at 0.2 strain. Importantly, we can notice that the stability of the "Annealed 14 μm GS", and "63Cr-800-1 0.6 μm GS" steels is quite equal up to 0.25 strain.

In the Nohara equation (Equation (1)) for M_{d30}, the coefficient of N is 462, which means that the change of 0.022%N would cause the change of 10 °C in M_{d30}. However, during the reversion GS has been refined from 20 to 0.6 μm (ASTM8 to ASTM18). According to Equation (1), this GS refinement reduces M_{d30} by 1.42 × 10 = 14 °C (i.e., M_{d30} changes from 27 to 13 °C). Additionally, the M_{d30} difference of 10 °C between the steels based on the chemical compositions must be accounted, i.e., the total difference is 24 °C. With the power of 462 for N, the change of 0.052%N can cause this. This is about 1/3 of the total content of 0.15%N in the steel. Thus, we can conclude that binding of a part of N, which was available (0.15%) in the 301LN ASS studied by Järvenpää et al. [84,85,87,102], was good enough to result in the considerable stability drop, seen in Figure 11, observed between the low-temperature (precipitated) and high-temperature (no precipitates) annealed structures of this steel.

5.2.3. Elongation, Stacking Fault Energy and Deformation Mechanism

The M_{d30} temperature and SFE are relevant parameters concerning the mechanical stability of austenite towards the martensitic phase transformation. M_{d30} temperature was discussed in Section 2. It is commonly pointed out, that the SFE of a material determines the deformation mechanism and thereby affects the strain hardening behavior and ductility. The contribution of DIM formation to ductility was discussed earlier concluding that too a high fraction of DIM is not beneficial.

It is well known that a low SFE (≤20 mJ/m^2) favors the martensitic transformation (TRIP effect), whereas a higher SFE favors mechanical twinning (TWIP effect), e.g., [168]. Saeed-Akbari et al. [169] presented 20 mJ/m^2 as the upper limit for strain-induced α′-martensite formation in high-Mn steels. Allain et al. [168] suggested that with the SFE in the range 12–35 mJ/m^2, mechanical twinning would take place in addition to dislocation glide. It is well known that for instance in medium-Mn steels, the best combination of strength and ductility is obtained when both the TWIP and TRIP effects are activated in austenite grains, e.g., [170]. There are opinions that twinning plays a vital role in contributing to the excellent ductility of reversion-treated effectively grain-refined ASSs [90,149,171], where the DIM formation becomes restricted due to fine GS.

SFE of ASSs has been discussed for instance by Lo et al. [110]. Recently Noh et al. [115] considered the validity of several equations proposed in the literature for determining the SFE of ASSs and the influence of SFE on the thermal and mechanical stability of austenite. They found that the tendency for strain-induced martensite transformation was governed not by the thermodynamic stability but by the SFE, which was increased more effectively by Ni than by the equivalent amount of Mn. They developed a modified SFE equation (Equation (4)) and experimentally determined Ni equivalents which may provide a criterion for austenite stability under tensile deformation.

$$\text{SFE (mJ/m}^2\text{)} = 5.53 + 1.4[\text{Ni}] - 0.16[\text{Cr}] + 17.1[\text{N}] + 0.72[\text{Mn}], \quad (4)$$

Here the alloying elements are in mass %. Using Equation (4), the SFE of 20 mJ/m^2 was found to be the limit for stable austenite against DIM formation; hence, the same value as suggested to be the upper limit for martensite formation earlier [168,169]. For the 301LN steel used by Somani et al. [23] (see Table 1), the predicted SFE is 15.36 mJ/m^2, a value in fair agreement with that determined experimentally by Talonen (13–15 mJ/m^2) [155].

Equation (4) does not include the GS, but it is also known that in addition to temperature, fine GS increases the effective SFE [167,169]. The effective SFE is affected by grain boundaries tending to decrease the width of extended dislocations (see e.g., Mahato et al. [172]). It can be estimated from the work of Saeed-Akbari et al. [169]) that the submicron GS in reversed microstructures tends to increase the SFE of Cr-Mn and Cr-Ni ASSs by about 6 mJ/m^2. Hence, when the SFE of 301LN is 15 mJ/m^2, in a highly refined structure, the effective SFE could be 21 mJ/m^2. This is above the limit value of 20 mJ/m^2, and DIM formation might be restricted. Anyhow, we can conclude that refined GS reduces the DIM formation tendency and favors the activation of the TWIP effect instead of TRIP. This supports the arguments of Misra et al. [25,90,171] concerning the role of twinning in grain-refined ASSs.

Xu et al. [20] reported the occurrence of mechanical twinning instead of DIM in an 18Cr-8.3Ni ASS with the predicted SFE of 18.9 mJ/m^2 without accounting for any GS (≈2 μm) influence. We can conclude that the effective SFE has been about 25 mJ/m^2 for the grain-refined steel so that DIM formation is expected to be negligible. Lei et al. [51] found both TRIP and TWIP mechanisms in ultrafine-grained (GS 0.22 μm) 17Cr-6Ni-2Cu steel with the calculated SFE of 16.4 mJ/m^2 (using Noh's equation (Equation (4)) SFE is 12.6 mJ/m^2 without effects of GS and Cu, but both of them increase the SFE), so the existence of twinning is expectable. Hamada et al. [156] reported that the highest tensile elongation was achieved in coarse-grained 201 and 201L ASSs at 50 °C, where both the TRIP and TWIP effects were found to be active, apparently due to increase of the SFE by elevated deformation temperature. The SFE of the studied steels was estimated to be in the order of 20 mJ/m^2 at 50 °C.

In summary, it seems that the SFE of slightly below 20 mJ/m^2 is quite optimal for strain hardening, while twinning may contribute to high ductility with minor DIM formation in Cr-Ni and Cr-Mn ASSs. Thus, in principle the GS refinement affects beneficially the SFE of 301, 301LN and 304 steels while increasing it.

5.2.4. Strain Hardening Rate and Elongation

If we compared the SHR affected by DIM formation and the respective elongation in a tensile test, it is obvious that the elongation is not directly related to the maximum SHR or DIM fraction (Figure 12a). The latter fact was also pointed out earlier as an observation that the maximum elongation generally corresponds to DIM fractions below 20%. However, it seems that we can find a relationship between the tensile elongation (fracture strain) and the strain corresponding to the maximum SHR (called a peak strain), as demonstrated in Figure 12b. The figure includes data from tensile tests at different temperatures [154–156] and different grain sizes [83,85,102]. In both instances, the elongation increases with the increasing peak strain. From the relationship, it can be concluded that the maximum SHR should be reached as late as possible to delay necking (though before necking), and generally the DIM formation tends to occur too early, at too small strains. According to the data in Figure 12b, there are no cases where the austenite is too stable (concerning the ASS grades 201, 201LN, 204Cu, 301 and 301LN). Consistently, in medium-Mn steels with duplex structure, superior mechanical properties are obtained when the volume fraction and stability of austenite are maximized [170].

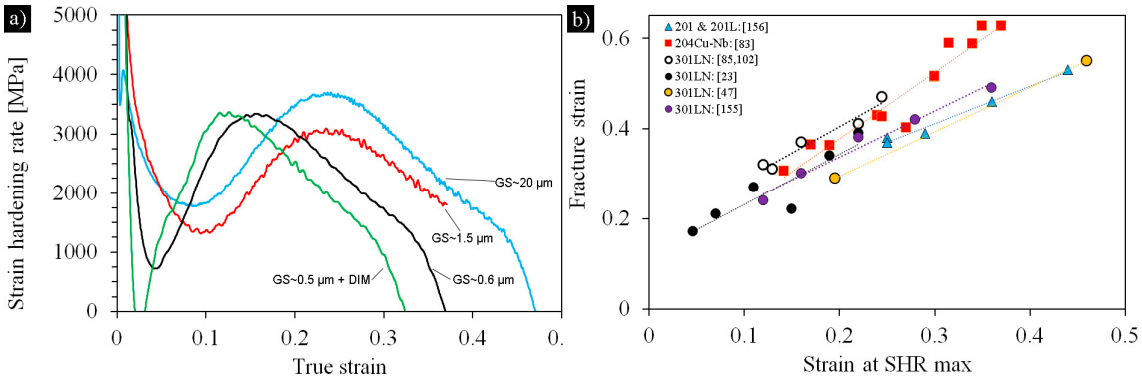

Figure 12. Strain hardening rate curves for selected AISI 301LN structures [85,87] (**a**) and the relation between fracture strain and the strain at the peak SHR (**b**). SHR = strain hardening rate.

Considering the reason for the SHR exhibiting a peak, according to Marechal [75], the kinetics of austenite to martensite phase transformation dominates at the strains before the peak, whereas at the peak and beyond, the apparent work hardening of the α'-martensite has the dominant effect on SHR. Thus, the rate of DIM formation should not be too fast but gradual.

5.2.5. Discontinuous Yielding

Discontinuous yielding, Lüders strain, has been frequently observed in ultrafine-grained ASSs [51,80,85,87,160,173]. Conventionally, the yield point is connected with a high density of mobile dislocations formed by unlocking pinned dislocations and rapid dislocation multiplication, when the material within the deformation band effectively softens and undergoes localized plastic deformation [174,175]. Lüders-type behavior has been detected in an ultrafine-grained Fe-C alloy with carbide particles [176] and Matsuoka et al. [160] reported it in 16Cr-10Ni ASS with 1 μm GS. Lei et al. [51] found a Lüders strain of 15% in an Fe-0.06C-17Cr-6Ni-2Cu with GS ≈ 220 nm. The appearance of a yield point with low subsequent strain hardening also happens in austenitic TWIP-type steels in connection with GS refinement down to a few microns [177].

Gao et al. [173] observed a very long Lüders strain of 0.4 in tensile deformation of an ultra-fine grained (bimodal GS, 1 μm and 0.2 μm) 304 ASS fabricated by a two-step cold rolling and annealing process. The authors explained the observation by intense formation of martensite, promoted by the incremental strain localization in the band region. After that, the strain localization region started to propagate to the undeformed region, leading to the Lüders-type deformation and also the high subsequent uniform elongation. Marechal [75] demonstrated the presence of 24% stress plateau in a stress–strain curve of a 301LN, cryorolled (100% DIM) and annealed at 750 °C for 30 min, forming a partially recrystallized fine grain structure without DIM.

Järvenpää et al. [29,87] showed that the discontinuous yielding in a 301LN ASS became more pronounced with decreasing GS obtained with decreasing annealing temperature so that the Lüders strain disappeared when the GS was larger than about 1 μm, and the annealing temperature increased to 900 °C. Typical stress–strain curves revealing that are displayed in Figure 13. At 690 °C the reversed GS is below 1 μm and Lüders strain of even more than 10% appears, though dependent on the presence of retained phases DIM and DA and the fraction of fine grains (affected by the prior cold rolling reduction).

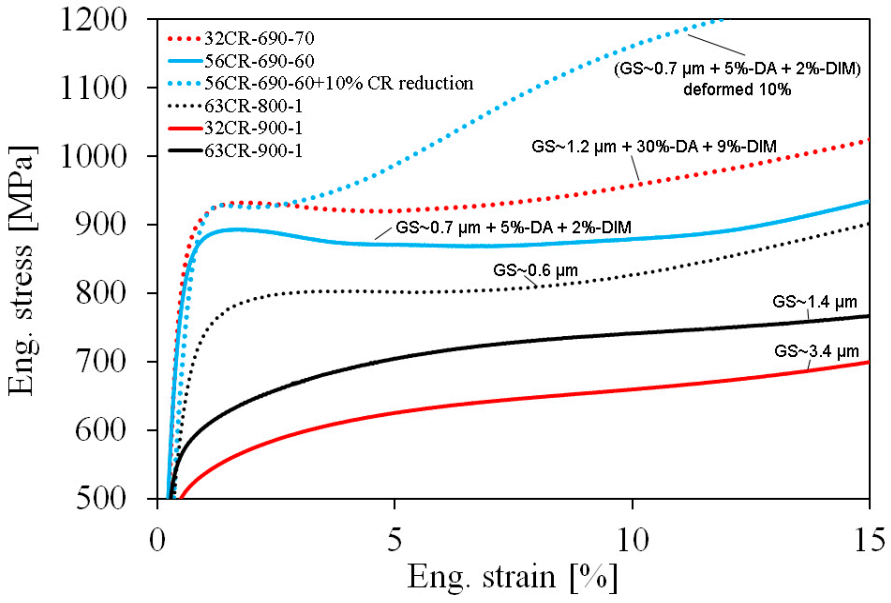

Figure 13. Initial parts of stress–strain curves of various reversed structures of a 30LN steel. Data from References [29,87]. Legend: Reduction (%CR), temperature (°C), duration (s).

Thus, the discontinuous yielding phenomenon in 301LN ASS could be connected with effective GS refinement or/and precipitation occurred at low annealing temperatures. Järvenpää [102] suggests that in addition to submicron-sized GS, the imposing softening and Lüders-type yielding are enhanced by the interaction between dislocations and fine precipitates, i.e., pinning effects. Marechal [75] explained

and modelled the appearance of the discontinuous yielding with two factors: DIM formation at small strains (transformation strain contribution) and, as a key factor, the relative flow stress difference between work hardened fine-grained austenite and DIM, resulting in a negative strain hardening rate contribution balancing the influence of the work hardening of austenite. Accordingly, when the GS of austenite is sufficiently reduced to increase its strength and the transformation rate of DIM is also sufficient (affected possibly by the precipitation in a 301LN), though not particularly high, the strain localization will be induced.

At any rate, the discontinuous yielding of a partially reversed structure can be largely diminished by subsequent 10% cold rolling reduction, as demonstrated in Figure 13 [87]. Obviously, new mobile dislocations are created by this plastic deformation.

5.2.6. Tensile Properties of Temper-Rolled Reversed Structures

As mentioned, temper rolling is a common method to improve the strength of annealed ASSs. The influence of small cold rolling reductions on the tensile properties of reversed structures of 301LN grade has rarely been investigated. However, in a study [87], it was found that a 10% cold rolling reduction increased the YS of the low-temperature annealed (690 °C–60 s) structure only faintly (see Figure 13), although the DIM fraction grew by 10%. A 20% reduction increased the YS slightly more efficiently, but the improvement, in spite of 38% DIM, was still very modest in comparison with the effect of the same cold rolling reduction on a commercial steel containing 29% DIM. It is obvious that the influence of the DIM formation on the strength is more pronounced in a soft coarse-grained structure than in a strong reversed structure, but also the work-hardening of the soft coarse austenite grains must be much higher than the work-hardening of refined reversed grains.

Mao et al. [178] have recently reported that a good combination of strength and ductility can be obtained in a fine-grained (average GS 5 μm) 316L ASS by a cold rolling reduction of 30%. The steel sheet exhibited the YS and TS of 1045 and 1080 MPa, respectively, but with a short uniform elongation of 7%. Jung and Lee [179] applied warm rolling of 40% reduction at 500 °C to a 10.30Cr–8.14Ni-7.41Mn ASS, previously 75% cold rolled and annealed at 663 °C for 5 min to obtain a fine GS of 2 μm. This deformation increased the YS from 401 to 736 MPa (TS 1076 MPa, TE 25%). This observation on a significant improvement of the YS is somewhat different from those of Järvenpää et al. [87], but the rolling reduction used was also much higher.

5.3. Fatigue Behavior

5.3.1. Fatigue Strength

The effect of the GS refinement on fatigue strength has been studied extensively in nano-structured materials and also in metastable ASSs [43,60,64,74,87,180–196]. GS can be refined by various means in addition to the reversion, too. For instance, Ueno et al. [181] used equal channel angular pressing to obtain nanosized grain structure in a 316L ASS and observed a beneficial effect of GS refinement on fatigue strength. A drastic enhancing influence of nanocrystalline structure created by an ultrasonic attrition treatment has been reported for 316L and 301LN ASSs in bending fatigue cycling [185]. In this instance, in addition to the refined GS, compressive residual stresses and DIM formation during the attrition treatment can contribute to the fatigue strength improvement.

Examples of the results of the studies on the fatigue strength of reversion-treated ASSs are plotted in Figure 14, the strain amplitude–fatigue life curves in Figure 14a and the stress amplitude–fatigue life curves in Figure 14b. The influence of GS is not pronounced as based on strain amplitude (Figure 14a) compared to that if based on stress amplitude (Figure 14b). Di Schino et al. [43] investigated the high cycle fatigue (HCF) behavior of the N-alloyed (16.5Cr-1.0Ni-11.5Mn-0.3N) steel in axial load-controlled tests as a function of the GS, but they did not found any influence of grain refinement on the fatigue limit (2×10^6 cycles). This was explained in terms of the formation of slip bands on the steel surface

promoted by nitrogen alloying and crack initiation in them. On the contrary, a slight beneficial effect of GS refinement was detected in the fatigue limit of a standard 304 ASS, as seen in Figure 14b.

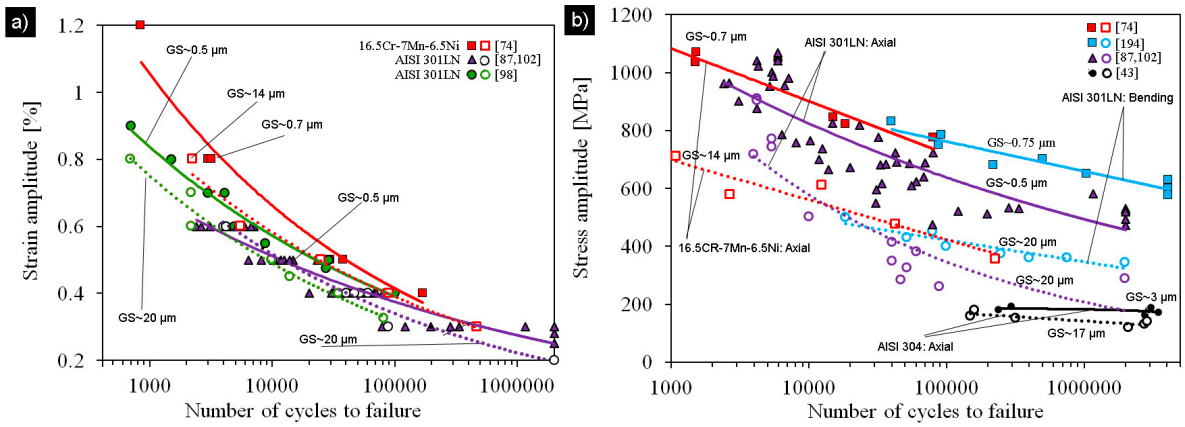

Figure 14. Fatigue life of reversion-treated 301LN in total strain-controlled tests compared to coarse-grained or annealed steel based on (**a**) strain amplitude and (**b**) mid-life stress amplitude. Data for 304 and 16.5Cr-7Mn-6.5N are from References [43] and [74], respectively.

Hamada et al. [194] noticed a significant improvement in the fatigue life of a reversion-treated 301LN steel (63% cold rolling reduction, annealing at 800 °C for 1 s; average GS ~0.75 μm) under bending fatigue loading compared that of the coarse-grained (GS ≈ 20 μm) counterpart (number of cycles to fracture more than 10^4 cycles). As evident from Figure 14b, the fatigue limit was significantly increased from 350 MPa to 630 MPa, reaching 59% of the TS. Planar dislocation structure typical to low SFE metals was found in fatigued coarse-grained steel, with intense formation of slip bands and crack propagation along these bands and grain boundaries. Contrary to that, fatigue loading created few deformation features, and fatigue damage was observed to occur by grain boundary cracking in the fine-grained counterpart. A small amount of DIM was formed in the fine-grained structure, whereas in the coarse-grained steel, appreciable amount of martensite was detected, and hardness increased about 47% during cycling. It should be noted that due to a high cycling frequency of 23 Hz, specimens tended to be heated during fatigue loading, which may have affected the austenite stability. Due to higher strength of the fine-grained steel, the adiabatic heating might be higher in fine-grained than in coarse-grained specimens.

Fargas et al. [64] carried out axial fatigue tests with a 301LN ASS under load control (R = 0.1) and found that GS refinement achieved by reversion treatments led to fatigue limits clearly higher than that of annealed coarse-grained counterpart. Interestingly, even a 20% cold rolling reduction providing 28% DIM was enough for this improvement. They also observed that after the fatigue tests, the amount of DIM was close to 44% for the coarse-grained (GS 11.7 ± 4.1 μm) steel, while the reverted samples (40% cold rolling reduction before annealing and GS 2.3 ± 1.5 μm) showed less than 23% of DIM. Hence, the stability of austenite increased with decreasing GS and less slip bands were also observed in fine-grained structures, both observations being consistent with those by Hamada et al. [194].

Liu et al. [182] used the tension-tension loading (R = 0.2 at 95 Hz) for an 18Cr-8Ni ASS (70% cold rolling; annealing 710 °C–10 min, 760 °C–5 min and 950 °C–5 min). They obtained the fatigue strengths of 811, 568 and 501 MPa for the reversion-treated structures with GS of 400 nm, 1.4 μm, and 12 μm, respectively, i.e., a distinct improvement in fatigue strength due to the GS refinement. The respective YS values were 878, 571 and 316 MPa so that the fatigue strength was lower than the YS for submicron-grained steel but higher for the coarse-grained one. After fatigue testing, distinct slip bands were formed on the surface of the coarse-grained sample, while shallower slip bands were present on fine-grained surfaces. The surface of the submicron-grained sample was smooth and without slip bands or other deformation marks. This sample also showed the smallest increase in hardness in

fatigue, only 8%, whereas the hardness increased up to 80% in the coarse-grained counterpart. In the submicron-grained structure, a very small amount of martensite and dislocations were generated. Moreover, these observations on surface deformation and the higher stability of the refined structure are in agreement with those reported earlier by Hamada et al. [194] and Fargas et al. [64] for 301LN ASS.

In strain-controlled fatigue testing, nano- or ultrafine-grained materials usually exhibit longer fatigue lives in the HCF regime and shorter fatigue lives in the LCF regime compared to their coarse-grained counterparts due to their higher strength and lower ductility, respectively (see e.g., Höppel et al. [180]). However, as shown in Figure 14a, Man et al. [184,196] and Chlupova et al. [99] reported slightly higher fatigue resistance of the ultrafine-grained structure compared to that of coarse-grained counterpart of a 301LN ASS in the range 10^4–10^6 cycles. Moreover, Droste et al. [74] reported an improvement of the fatigue life due to the GS refinement (from 28 to 0.7 μm) both in LCF and HCF regimes in a metastable 16.5Cr-6.5Ni-7Mn ASS under total strain amplitude loading. They suggested that the small difference in hardness between austenite and DIM in the ultrafine-grained partially-reversed structure would lead to more homogeneous strain distribution during cycling, whereas in the coarse-grained structure, strain is localized in the austenite phase. The data of Järvenpää et al. [87,102] also inserted in Figure 14a, indicate hardly any influence of GS on the LCF life of the same steel. However, in a comparison based on the mid-life stress amplitudes, the reversed fine-grained structure was distinctly better than the coarse-grained counterpart (Figure 14b). In the HCF regime, the fatigue strength, i.e., the stress amplitude level at 10^6 cycles, was in the range of 460–570 MPa for the reversed structures (GS ≈ 0.6–3.4 μm), being even more than twice higher compared to corresponding value of the annealed coarse-grained (≈20 μm) structure.

Järvenpää et al. [29,87] have shown that low prior cold rolling reductions before the reversion annealing can lead to fatigue strength identical to that achieved after the 63% reduction. For the highest fatigue, strength of over 500 MPa was obtained in the partially reversed 32% and 56% cold-rolled structures created at lower temperatures with longer holding times. The fatigue strength was practically independent of the loading direction relative to the rolling direction. Mateo et al. [190] reported that even a cold rolling reduction as low as 20%, resulting in a very non-homogeneous reversed structure (the mean GS below 3 μm), led to 36% improvement (i.e., 100 MPa) of the fatigue limit compared to that of an annealed 301LN. However, the fatigue limit remained lower than that of a 20% temper-rolled sheet.

Similarly, as in the case of tensile properties, subsequent cold rolling deformation has been found to have only a slight effect on the fatigue strength of the partially reversed structure in a 301LN ASS, whereas the improvement is much more pronounced in the coarse-grained steel [87,102]. However, the fatigue limit (at 10^6 cycles) for the low-temperature reversed structure is about 600 MPa without any temper rolling, corresponding to the fatigue limit of 20% temper-rolled coarse-grained structure.

In summary, it can be noticed that the fatigue strength of reversion-treated ASSs has been extensively studied for Cr-Ni and few Cr-Ni-Mn grades. Research on Cr-Mn type steels seems to be lacking. The results indicate the fatigue strength is highly improved by the GS refinement, as compared on the basis of stress amplitude. As is typical, the comparison based on strain amplitude does not show significant influence of GS. The influence of GS can be seen in the formation of slip bands and crack initiation.

5.3.2. Cyclic Stability

In metastable ASSs DIM forms during tensile testing and also during fatigue loading. Hard martensite in the soft austenitic matrix is known to improve fatigue strength; e.g., [60,64,98,186–192]. The cyclic deformation-induced martensitic transformation depends on the temperature, total strain amplitude and the cumulated plastic strain [186], and significantly on GS as pointed out in the previous section.

It has been shown that an increase in the DIM fraction leads to higher fatigue strength in the HCF regime due to increased strength, but relatively, LCF strength is decreased due to impaired ductility. It has been argued that there is an upper limit to martensite fraction in improving the fatigue resistance in the HCF regime, but the exact value of this limit seems to be unclear. Topic et al. [191] showed that in a 304 ASS (coarse-grained condition), pre-formed DIM is beneficial for fatigue life if its fraction is below 20%. Mateo et al. [60,190] found that even a 28% DIM fraction did not impair fatigue strength and Fargas et al. [64] reported a clear improvement even with a 38% DIM fraction (obtained by 40% reduction of a coarse-grained annealed sample) in cold rolled specimens.

Initial cyclic softening followed by pronounced cyclic hardening has been observed in cyclic loading in a coarse-grained annealed 304 ASS. The cyclic hardening is connected with DIM formation during dynamic straining, e.g., [192]. Poulon et al. [195] observed in a 15.38Cr-9.06Ni-3.06Mo ASS, with a fine 2.5 μm and coarse 21 μm GS, a slight cyclic softening followed by a secondary cyclic hardening, whatever the GS. The secondary cyclic hardening was more intense and started earlier at high strain amplitudes, being promoted especially in the coarse-grained steel. During the hardening stage, in grains larger than 2 μm, the formation of DIM occurs inside austenite grains on dislocation structures with the presence of nuclei on cell walls or dipolar walls. However, in fine grains, where plasticity activity occurs at grain boundaries, an intragranular dislocation structure is not a prerequisite for martensite nucleation but nuclei can appear along grain boundaries.

Biermann et al. [186] and Droste et al. [74] divided cyclic behavior of a 16.5Cr-7Mn-6.5Ni ASS into three stages: a primary hardening followed by a stage of cyclic softening being related to an increasing dislocation density and their interactions in the beginning of cyclic deformation and a rearrangement and annihilation of dislocations in the stage of cyclic softening and, finally, a secondary hardening due to the martensitic transformation. The secondary hardening increases with increasing strain amplitudes, and the onset occurs at a lower number of cycles. Increasing temperature reduces the degree of secondary hardening. In a recent study, laser beam annealing has been used to reverse the DIM in this steel, and cyclic hardening behavior and fatigue properties investigated [193]. Earlier, laser annealing was used for the reversion in a 301LN steel [197].

In studies of Järvenpää et al. [84,87], Chlupova et al. [99] and Man et al. [196], a minimal softening was found in reversed structures of a 301LN ASS at a strain amplitude of 0.4%, as seen in in Figure 15a. The same has reported by Droste et al. [74] for a 16.5Cr-7Mn-6.5Ni ASS. The softening was followed by slight hardening of the coarse-grained structure. At a higher total strain amplitude of 0.6%, both the coarse-grained and fine-grained reversed structures experienced unstable behavior, characterized by a pronounced hardening period, as illustrated in Figure 15a. A slight softening took place before that in the fine-grained structure, but not in the coarse-grained counterpart. However, the fine-grained reversed structures, which were strong as shown by the stress amplitude level (initially about 750 MPa), exhibited much less cyclic hardening than the coarse-grained structure, which had a low initial stress amplitude (about 320 MPa). Therefore, the stress amplitudes were close to each other after about 5000 cycles. DIM transformation occurred over the course of cycling after certain incubation periods (Figure 15b), and obviously, this is connected with cyclic hardening. However, in spite of a very different amount of hardening between the structures with these different GSs, the amount of DIM formed in cycling was high but quite similar among the studied structures (about 80% DIM after 5000 cycles at 0.6%). Thus, the influence of GS on DIM formation was not pronounced, which is somewhat contrary to the observations from load-controlled tests mentioned in the previous section. However, the influence of a given DIM fraction on cyclic hardening is much more significant in soft coarse-grained austenitic structure than in strong fine-grained structure, similarly as reported by Droste et al. [74]. Järvenpää et al. [84] have discussed this.

In summary, after initial slight softening or constant stage, cyclic hardening takes place in grain-refined as well as coarse-grained ASSs, which can be attributed to DIM formation. The amount of DIM is independent of the GS, but the degree of cyclic hardening is more pronounced in soft

coarse-grained austenite than in grain-refined austenite. The background of the phenomena is quite well understood.

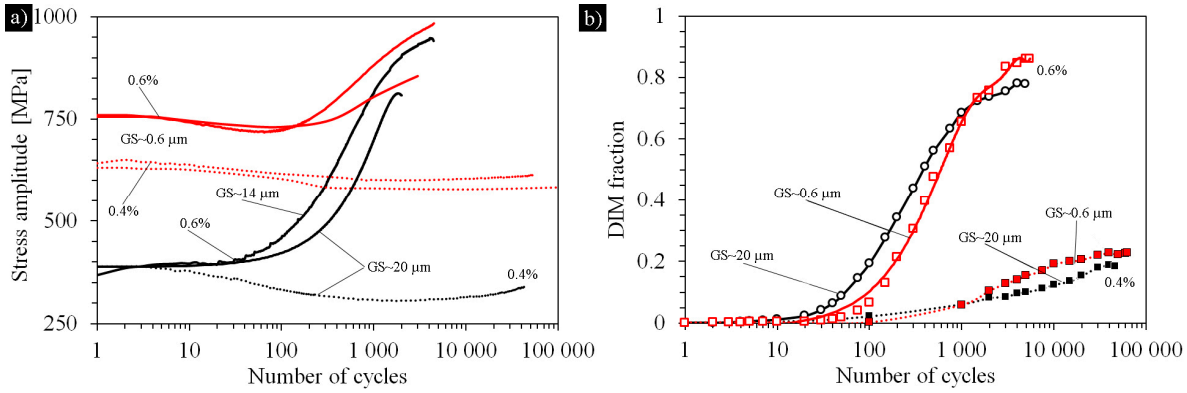

Figure 15. Cyclic medium-life stress amplitude (**a**) and DIM fraction (**b**) vs number of cycles curves of coarse-grained and reversed fine-grained 301LN at 0.4% and 0.6% strain amplitudes. Data from References [87,99,102].

5.4. Stretch Formability

The formability properties of reversion-treated structures are scarcely reported in the literature. Tensile ductility of ASSs is high, so the formability can be expected to remain on a good level in spite of the GS refinement and high strength. In one study, the stretch formability properties of the reversion treated 3 mm thick sheets of a 301LN ASS with the YS in the range 682–998 MPa, and temper-rolled structures of 301LN and 301ASSs, for reference, have been determined by the Erichsen cupping tests [198]. The results indicated that the stretch formability of the reversion-treated structures is identical or slightly better than that of the temper-rolled counterparts at a given YS level. Furthermore, the stretched cup surface of reversion-treated sheets is smoother than the surface of the cups of commercial temper-rolled sheets. This is in accordance with a technical data from Nippon Steel & Sumitomo Metal reporting excellent strength and formability for grain-refined thin sheets of AISI 304 (SUS304 BA1) and 301L (NSSMC-NAR-301L BA1) [108,109]. Further tests on the formability have been carried out by the authors but not published yet, and the study continues.

5.5. Weldability

Welding of steel sheets is often needed for constructive applications. In fusion welding processes, cold-strengthened ASSs tend to soften at the heat-affected zone (HAZ), and therefore, welding with restricted heat inputs must be applied. Weldability of reversion-treated ASSs has been investigated very scarcely. In a very recent study [199], it has been shown that autogenous laser welding of a reversion-treated ultrafine-grained (YS ~ 670 MPa) 301LN steel sheet (3 mm thick) created a weld metal with coarse columnar grains and a very narrow HAZ, similarly as happens in a temper-rolled (YS ~ 740 MPa) sheet [200–202]. Figure 16 displays an example of a laser welded joint and its microstructure and hardness distribution in a 3 mm 301LN steel. The weld metal has a low hardness (240 HV), naturally identical in the both sheets corresponding to the hardness of a hot-rolled sheet. The HAZ in the reversion-treated sheet exhibited grain coarsening, but in the temper-rolled counterpart, the GS is locally refined due to the recrystallization of the cold-rolled structure [201,202]. However, the grain structure of the HAZ was still finer in the reversion-treated sheet and the softened zone was slightly narrower. The YSs determined of the specimens cut across the weld seams were equal (629 MPa), but the elongation was clearly better in the seam of the reversion-treated sheet. The YS of the laser welded sheets was about double compared to that (330 MPa) of the hot rolled AISI 301LN sheet. However, the fatigue limits were quite equal in the hot rolled and laser-welded reversion-treated and laser-welded temper-rolled sheets.

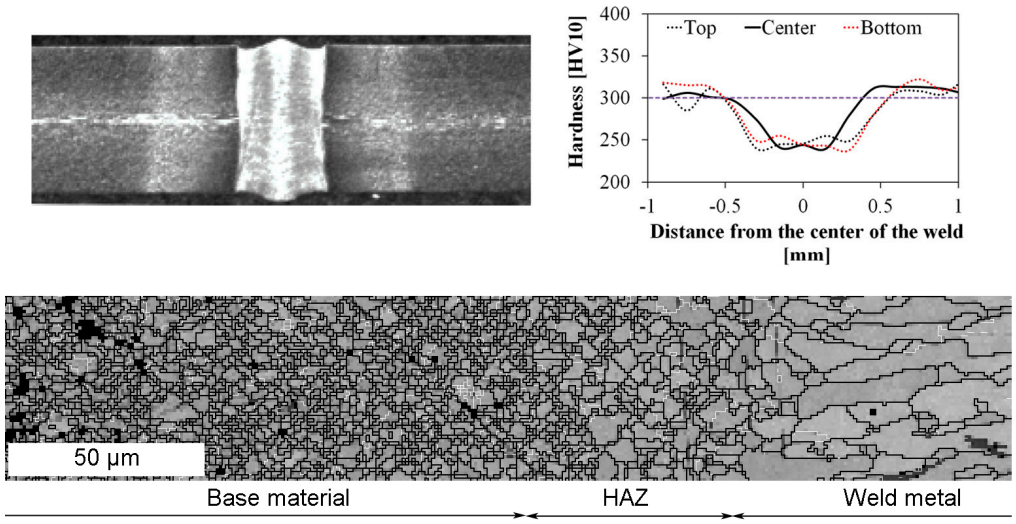

Figure 16. Cross-section of a laser weld on a reversion-treated 301LN sheet, hardness profile and grain size distribution. The hardness profile is from Reference [199].

5.6. Corrosion Resistance

High corrosion resistance is one of the most important properties of ASSs. Lv et al. [203] have investigated the effect of cold rolling temperature in the range from −196 °C to RT on corrosion resistance of a 304L ASS by potentiodynamic polarization tests in a borate buffer solution. In rolling, the austenitic microstructure was transformed completely to martensite. Results showed that samples cold rolled at −120 °C had an equiaxed GS of about 300 nm, which displayed the best corrosion performance. Moreover, the reverse transformation treatment was performed by annealing at 850 °C for 180–270 s, but no results were given concerning the reversed structures.

Han et al. [204] showed that a refinement of austenite GS of a 304 ASS strip by a thermomechanical treatment improved the TS and particularly the YS and also increased the intergranular corrosion resistance. This was explained as a result from the increased grain boundary area and thereby a decreased degree of the Cr depletion caused by carbide precipitation in the steel.

Di Schino et al. [41,42] have investigated the effect of refined GS on various properties of a low-Ni nitrogen alloyed Cr-Mn (Fe-0.037C-18.5Cr-1.07Ni-11.4Mn-0.37N) ASS. In the experiments, cold rolling of 75% reduction created about 45%DIM, and after the reversion annealing at 900 °C, GS varied from 2.4 µm after 10 s to 3 µm after 10 ks holding. The general corrosion rate of the ASS with 2.5 to 40 µm GSs was measured in 5% H_2SO_4 boiling solution for 10 h. It was found that the corrosion rate increases with decreasing GS. It was concluded that increasing the grain boundary surface area by grain refining causes destabilization of the surface passive film. The intergranular corrosion rate was estimated by immersing the samples in H_2SO_4 -$FeSO_4$ (Streicher solution) for 10 h. The intergranular corrosion rate was found to decrease with decreasing GS. As GS is refined, the grain boundary area per unit volume increases and the degree of the Cr depletion caused by carbide precipitation will decrease for a given carbon content. The pitting corrosion rate was measured in a 10% $FeCl_3$-$6H_2O$ solution at RT for 10 h. In contrast to the reduction of the general corrosion resistance, the grain refining led to improved pitting corrosion resistance in the low Ni-nitrogen alloyed steel as well as in a 304 ASS used for the reference. The pitting of ultrafine grained steel was found to initiate in several sites but with small individual pits, whereas in the large-grained steel pits were coarse and deep though lower in number. Moreover, the pitting potential was found to shift towards more noble potentials with decreasing GS.

Consistent with the result of Di Schino et al. [41,42], also Hamada et al. [205] reported that in a 301LN ASS the submicron-grained structure, formed upon reversion annealing at 800 °C for 1 s, exhibited a better pitting corrosion resistance than the coarse-grained structure. This was attributed to the preferential and faster pitting attack on grain boundaries in the coarse-grained steel,

presumably due to more severe impurity segregation or chromium-nitride precipitation than in the ultra-fine-grained structure.

As discussed in Section 5.2.2, precipitation of tiny Cr_xN particles has been detected in 301LN ASS, occurring presumably in DIM before the reversion at 600–800 °C [22,26]. Hence, some concern can arise if the precipitation impairs the corrosion resistance, even though the improvement in intergranular corrosion resistance was reported [41,42], as mentioned above. The unpublished research on this issue performed at the University of Oulu has indicated that there exists no risk to intergranular corrosion in the instance that no DIM is present, i.e., after complete reversion. Electron microscopy studies have revealed that particles locate inside austenite grains, not along grain boundaries [22,26,86], obviously due to precipitation in deformed martensite before its transformation. However, the presence of more than 2.7% DIM seems to degrade the corrosion resistance of low-temperature reversed structures. According to the Strauss test, sensitization also in a 204Cu ASS has been found possible after reversion annealing at 700 °C for 100–200 s (the DIM content 2.5% to 3%).

In summary, the general corrosion resistance is impaired, but the pitting corrosion resistance is improved by refined GS. Retained DIM may be detrimental for corrosion resistance, and some concern exists regarding the sensitization of ASSs with nitrogen alloying or high carbon content. Further investigations might be performed to further clarify the issue.

5.7. Properties for Medical Applications

Additionally, metals or alloys with nano- or ultrafine-grained structures are attractive materials for biomedical applications. Higher strength is one property desired and can be increased by the reversion treatment, but also, their osteoblast activity seems to be improved by the GS. To enhance osseointegration of orthopedic implants, the surfaces of implants, which are in direct contact with bone tissue, are of importance. If the implant surfaces provide a better environment for bone cell functions, then the integration of the implant with the juxtaposed bone tissue can be improved. By modifying biomaterial surfaces to possess features having nanophase topography, implant surfaces mimic the feature size of natural tissues, providing a more realistic niche to promote cellular functions on implant surfaces. It seems that a steel surface with nano-/submicron-sized GS is this kind of advanced topography without the risk of delamination as is the case with anodized oxide films, for instance. The favorable enhancement of osteoblasts functions and cellular attachment on nano-grained surface is attributed to ultrafine GS, i.e., the availability of greater open lattice in the position of high angle grain boundaries and high hydrophilicity.

Professor Misra's group together with researchers at the University of Oulu has investigated reversion-treated 301LN ASS for medical purposes [206–210]. For instance, Venkatsurya et al. [207] compared osteoblast response of grain boundary grooved and planar nano-/ultrafine-grained surfaces. Nune et al. [208] studied the influence of GS on osteoblast differentiation and mineralization. The determining role of grain refined structure on osteoblasts functions was fundamentally defined so that surface roughness and grain structure are the contributing factors that strongly influence protein adsorption on substrates and consequently cell attachment; proliferation and expression level of actin, vinculin and fibronectin [209]. Recently, the corresponding behavior of a 304 ASS has been investigated in another research group [211], and similar features as for the 301LN ASS have been reported.

Tufan et al. [212] obtained by machining substantial grain refinement up to 98.2 nm on the 316L ASS surfaces. Biological experiments showed nearly 280% increase in the bone cell density on turned samples compared to the as-received 316L stainless steel at the 5th day of culture, which was explained with enhanced hydrophilicity of the turned sample as a result from the combined effect of surface nanocrystallization and rougher nanoscale surface topography.

It is well known that a Cu-alloyed 304 ASS has antibacterial properties when Cu precipitates in surface layers and release Cu ions, e.g., [213,214]. In annealed condition, the strength properties of this steel are relatively low (YS ≈ 250 MPa), but they can, evidently, be improved by refining the GS by the reversion treatment, as shown for a 304 ASS in numerous studies. The Cu precipitation in

annealed austenite needed for creating the antibacterial property requires quite a long aging time, but it can take place at temperatures 650–800 °C [214]. At these temperatures, the grain growth in ASSs is negligible, as discussed in Section 4.1. Further, Cu precipitation in deformed DIM can be supposed to be a much faster process than in annealed austenite. Thus, the micron-scale reversed GS can be retained during the aging treatment. The study on this issue has just been finished, and the results will be published soon.

The integration of cellular and molecular biology with material science and engineering as described here provides a route to modulate cellular and molecular reactions in promoting osteoinductive signaling of surface adherent cells.

6. Conclusions

A large number of laboratory experiments have demonstrated that many commercial metastable Cr-Ni and Cr-Mn ASS grades can, even after a reasonably low cold rolling reduction (≈20% to 50%), be reversion treated in a temperature region of 600–900 °C for a desired short duration, and excellent yield strength-elongation combinations and high fatigue strength are obtained. The mechanical properties surpass those of temper-rolled sheets. Moreover, the formability, corrosion and biomedical properties are enhanced by the reversion treatment, although these properties have been much rarely investigated. Weldability issues are most scarcely covered yet. After this intense research, the topic of reversion phenomenon is quite matured and well understood, even though many details depend on the exact chemical composition of the steel and processing variables (cold rolling degree, annealing temperature, etc.) The highly refined grain size is the main factor for the enhanced properties, but also partly reversed structures with retained martensite and austenite can exhibit excellent strength-ductility combinations, although the grain size remains coarser and non-uniform. Numerous processing factors affect the properties so that they must be adjusted for the case sensitively and the robustness of the processing checked. However, studies demonstrate that the reversion processing route could be adopted industrially for manufacturing austenitic stainless steels with advanced properties.

Recently it has been reported that the reversion-treatment approach can be adopted also to high-Mn-TRIP steels. Various phenomena and features, found during the reversion treatment of ASSs and discussed in previous sections, can exist in high-Mn-TRIP steels (Mn > 15%), too. In cold rolling of certain Fe-Mn-C alloys, e-martensite can form and reverse in subsequent annealing [215,216]. In low-carbon high-Mn steels, two types of α′-martensite have been found to exist after cold rolling with retained austenite [217–220]. The reversion of α′-martensite takes place during annealing in two temperature ranges, together with a new phenomenon of Mn partition, not reported in the reversion stage in ASSs. Both shear and diffusional reversion mechanisms can occur, and GS refinement can be effective in austenite formed from cell-type martensite while ineffective in austenite reversed from lath-type martensite. During deformation, TRIP and also TWIP mechanisms can occur. Thus, this field is rich in details to be further investigated.

Reversion has been reported in high-entropy alloys [221], with the chemical composition metastable enough for deformation-induced martensite formation during cold rolling. This will expand the research field for studying reversion-affected phenomena and related properties.

Author Contributions: Conceptualization, data curation, draft preparation, A.J., M.J. and A.K.; visualization, A.J.; writing—review and editing, supervising, P.K. All authors have read and agreed to the published version of the manuscript.

Funding: This research was funded by the ACADEMY OF FINLAND, grant number 311934.

Acknowledgments: Outokumpu Stainless Oy is thanked for providing the commercial material and for long-lasting support for the reversion-related research at the University of Oulu.

Conflicts of Interest: The authors declare no conflict of interest.

Nomenclature

α	Parameter in Olson–Cohen model (Equation (3))
α'-martensite	Deformation-induced body-centered cubic martensite
β	Parameter in Equations (2) and (3)
ε-martensite	Hexagonal epsilon martensite
ε	Strain in Equations (2) and (3)
$\varepsilon_{m'}$	Abscissa of the mid-point of a sigmoidal curve (Equation (2))
σ_o	Friction stress in the Hall–Petch relation
A_f	Finish temperature of the martensite to austenite reversion
A_s	Start temperature of the martensite to austenite reversion
ASS	Austenitic stainless steel
CR	Cold rolling
DA	Deformed austenite, retained in cold rolling
DIM	Deformation-induced martensite (α'-martensite)
FCC	Face-centered cubic
$f_{\alpha'}$	Martensite fraction in Equation (2) and Olson–Cohen model (Equation (3))
f_s	Saturation martensite fraction in cold rolling deformation (Equation (2))
GS	Grain size
HAZ	Heat affected zone
HCF	High cycle fatigue
m	Exponent in Olson–Cohen model (Equation (3))
M_{d30}	Temperature where 50% a'-martensite is formed by 30% true strain
M_s	Starting temperature of martensite transformation
LCF	Low cycle fatigue
R	R ratio, minimum peak stress divided by the maximum peak stress in fatigue cycling
$R_{p0.2}$	Proof strength, yield strength
RT	Room temperature
SHR	Strain hardening rate
TE	Tensile elongation, fracture strain
TS	Tensile strength
YS	Yield strength

References

1. *Stainless Steel: Tables of Technical Properties*, 2nd ed.; Euro Inox: Brussels, Belgium, 2007; Volume 5, ISBN 9782879972428.
2. Mechanical behaviour and design values of properties. In *Design Manual for Structural Stainless Steel*; Euro Inox/The Steel Construction Institute: Brussels, Belgium; Chicago, IL, USA, 2006; p. 146. ISBN 2-87997-204-3.
3. Taulavuori, T.; Aspegren, P.; Säynäjäkangas, J.; Salmén, J.; Karjalainen, L.P. The anisotropic behaviour of the nitrogen alloyed stainless steel grade 1.4318. In Proceedings of the 7th High Nitrogen Steels Conference, Ostend, Denmark, 19–22 September 2004; pp. 405–412.
4. Karjalainen, L.P.; Taulavuori, T.; Sellman, M.; Kyröläinen, A. Some strengthening methods for austenitic stainless steels. *Steel Res. Int.* **2008**, *79*, 404–412. [CrossRef]
5. Mazza, B.; Pedeferri, P.; Sinigaglia, D.; Cigada, A.; Fumagalli, G.; Re, G. Electrochemical and corrosion behaviour of work-hardened commercial austenitic stainless steels in acid solutions. *Corros. Sci.* **1979**, *19*, 907–921. [CrossRef]
6. Barbucci, A.; Delucchi, M.; Panizza, M.; Sacco, M.; Cerisola, G. Electrochemical and corrosion behaviour of cold rolled AISI 301 in 1 M H_2SO_4. *J. Alloys Compd.* **2001**, *317–318*, 607–611. [CrossRef]
7. Mudali, U.K.; Shankar, P.; Ningshen, S.; Dayal, R.K.; Khatak, H.S.; Raj, B. On the pitting corrosion resistance of nitrogen alloyed cold worked austenitic stainless steels. *Corros. Sci.* **2002**, *44*, 2183–2198. [CrossRef]
8. Gavriljuk, V.G.; Berns, H.; Escher, C.; Glavatskaya, N.I.; Sozinov, A.; Petrov, Y. Grain boundary strengthening in austenitic nitrogen steels. *Mater. Sci. Eng. A* **1999**, *271*, 14–21. [CrossRef]
9. Simmons, J.W. Overview: High-nitrogen alloying of stainless steels. *Mater. Sci. Eng. A* **1996**, *207*, 159–169. [CrossRef]

10. Di Schino, A.; Barteri, M.; Kenny, J.M. Development of ultra fine grain structure by martensitic reversion in stainless steel. *J. Mater. Sci. Lett.* **2002**, *21*, 751–753. [CrossRef]
11. Di Schino, A.; Salvatori, I.; Kenny, J.M. Effects of martensite formation and austenite reversion on grain refining of AISI 304 stainless steel. *J. Mater. Sci.* **2002**, *37*, 4561–4565. [CrossRef]
12. Srikanth, S.; Saravanan, P.; Kumar, V.; Saravanan, D.; Sivakumar, L.; Sisodia, S.; Ravi, K.; Jha, B.K. Property Enhancement in metastable 301LN austenitic stainless steel through strain-induced martensitic transformation and its reversion (SIMTR) for metro coach manufacture. *Int. J. Metall. Eng.* **2013**, *2*, 203–213. [CrossRef]
13. Ravi Kumar, B.; Sharma, S.; Kashyap, B.P.; Prabhu, N. Ultrafine grained microstructure tailoring in austenitic stainless steel for enhanced plasticity. *Mater. Des.* **2015**, *68*, 63–71. [CrossRef]
14. Forouzan, F.; Najafizadeh, A.; Kermanpur, A.; Hedayati, A.; Surkialiabad, R. Production of nano/submicron grained AISI 304L stainless steel through the martensite reversion process. *Mater. Sci. Eng. A* **2010**, *527*, 7334–7339. [CrossRef]
15. Moallemi, M.; Najafizadeh, A.; Kermanpur, A.; Rezaee, A. Effect of reversion annealing on the formation of nano/ultrafine grained structure in 201 austenitic stainless steel. *Mater. Sci. Eng. A* **2011**, *530*, 378–381. [CrossRef]
16. Rezaee, A.; Kermanpur, A.; Najafizadeh, A.; Moallemi, M. Production of nano/ultrafine grained AISI 201L stainless steel through advanced thermo-mechanical treatment. *Mater. Sci. Eng. A* **2011**, *528*, 5025–5029. [CrossRef]
17. Sabooni, S.; Karimzadeh, F.; Enayati, M.H. Thermal stability study of ultrafine grained 304L stainless steel produced by martensitic process. *J. Mater. Eng. Perform.* **2014**, *23*, 1665–1672. [CrossRef]
18. Behjati, P.; Kermanpur, A.; Najafizadeh, A.; Baghbadorani, H.S. Effect of annealing temperature on nano/ultrafine grain of Ni-free austenitic stainless steel. *Mater. Sci. Eng. A* **2014**, *592*, 77–82. [CrossRef]
19. Baghbadorani, H.S.; Kermanpur, A.; Najafizadeh, A.; Behjati, P.; Rezaee, A.; Moallemi, M. An investigation on microstructure and mechanical propertiesof a Nb-microalloyed nano/ultrafine grained 201 austenitic stainless steel. *Mater. Sci. Eng. A* **2015**, *636*, 593–599. [CrossRef]
20. Xu, D.M.; Li, G.Q.; Wan, X.L.; Xiong, R.L.; Xu, G.; Wu, K.M.; Somani, M.C.; Misra, R.D.K. Deformation behavior of high yield strength—High ductility ultrafine-grained 316LN austenitic stainless steel. *Mater. Sci. Eng. A* **2017**, *688*, 407–415. [CrossRef]
21. Ma, Y.-Q.; Jin, J.-E.; Lee, Y.-K. A repetitive thermomechanical process to produce nano-crystalline in a metastable austenitic steel. *Scr. Mater.* **2005**, *52*, 1311. [CrossRef]
22. Rajasekhara, S.; Ferreira, P.J.; Karjalainen, L.P.; Kyröläinen, A. Hall-Petch behavior in ultra-fine-grained AISI 301LN stainless steel. *Metall. Mater. Trans. A* **2007**, *38*, 1202–1210. [CrossRef]
23. Somani, M.C.; Juntunen, P.; Karjalainen, L.P.; Misra, R.D.K.; Kyröläinen, A. Enhanced mechanical properties through reversion in metastable austenitic stainless steels. *Metall. Mater. Trans. A* **2009**, *40*, 729–744. [CrossRef]
24. Misra, R.D.K.; Nayak, S.; Mali, S.A.; Shah, J.S.; Somani, M.C.; Karjalainen, L.P. Microstructure and deformation behavior of phase-reversion-induced nanograined/ultrafine-grained austenitic stainless steel. *Metall. Mater. Trans. A* **2009**, *40*, 2498–2509. [CrossRef]
25. Misra, R.D.K.; Zhang, Z.; Jia, Z.; Somani, M.C.; Karjalainen, L.P. Probing deformation processes in near-defect free volume in high strength—high ductility nanograined/ultrafine-grained (NG/UFG) metastable austenitic stainless steels. *Scr. Mater.* **2010**, *63*, 1057–1060. [CrossRef]
26. Rajasekhara, S.; Karjalainen, L.P.; Kyröläinen, A.; Ferreira, P.J. Microstructure evolution in nano/submicron grained AISI 301LN stainless steel. *Mater. Sci. Eng. A* **2010**, *527*, 1986–1996. [CrossRef]
27. Kisko, A.; Hamada, A.; Karjalainen, L.P.; Talonen, J. Microstructure and mechanical properties of reversion treated high Mn austenitic 204Cu and 201 stainless steels, HMnS 2011. In Proceedings of the 1st International Conference on High Manganese Steels, Seoul, Korea, 15–18 May 2011; p. B-19.
28. Kisko, A.; Rovatti, L.; Miettunen, I.; Karjalainen, L.P.; Talonen, J. Microstructure and anisotropy of mechanical properties in reversion-treated high-Mn type 204Cu and 201 stainless steels. In Proceedings of the 7th European Stainless Steel Conference—Science and Market, Como, Italy, 21–23 September 2011.
29. Järvenpää, A.; Jaskari, M.; Karjalainen, L.P. Reversed microstructures and tensile properties after various cold rolling reductions in AISI 301LN steel. *Metals* **2018**, *8*, 109. [CrossRef]

30. Poulon-Quintin, A.; Brochet, S.; Vogt, J.-B.; Glez, J.-C.; Mithieux, J.-D. Fine grained austenitic stainless steels: The role of strain induced α′ martensite and the reversion mechanism limitations. *ISIJ Int.* **2009**, *49*, 293–301. [CrossRef]
31. Zhao, J.; Jiang, Z. Thermomechanical processing of advanced high strength steels. *Prog. Mater. Sci.* **2018**, *94*, 174–242. [CrossRef]
32. Smith, H.; West, D.R.F. The reversion of martensite to austenite in certain stainless steels. *J. Mater. Sci.* **1973**, *8*, 1413–1420. [CrossRef]
33. Smith, H.; West, D.R.F. Annealing of austenite formed by reversion from martensite in an Fe–16Cr–12Ni alloy. *Metals Technol.* **1974**, *1*, 37–40. [CrossRef]
34. Coleman, T.H.; West, D.R.F. Deformation-induced martensite and its reversion to austenite in an Fe–16Cr–12Ni alloy. *Met. Technol.* **1976**, *3*, 49–53. [CrossRef]
35. Guy, K.B.; Butler, E.P.; West, D.R.F. Reversion of bcc α′ martensite in Fe–Cr–Ni austenitic stainless steels. *Met. Sci.* **1983**, *17*, 167–176. [CrossRef]
36. Guy, K.; Butler, E.P.; West, D.R.F. Martensite formation and reversion in austenitic stainless steels. *J. Phys. Colloq.* **1982**, *43*, C4-575–C4-580. [CrossRef]
37. Singh, J. Influence of deformation on the transformation of austenitic stainless steels. *J. Mater. Sci.* **1985**, *20*, 3157–3166. [CrossRef]
38. Tomimura, K.; Takaki, S.; Tanimoto, S.; Tokunaga, Y. Optimal chemical composition in Fe-Cr-Ni Alloys for ultra grain refining by reversion from deformation induced martensite. *ISIJ Int.* **1991**, *31*, 721–727. [CrossRef]
39. Tomimura, K.; Takaki, S.; Tokunaga, Y. Reversion mechanism from deformation induced martensite to austenite in metastable austenitic stainless steels. *ISIJ Int.* **1991**, *31*, 1431–1437. [CrossRef]
40. Takaki, S.; Tomimura, K.; Ueda, S. Effect of pre-cold-working on diffusional reversion of deformation induced martensite in metastable austenitic stainless steel. *ISIJ Int.* **1994**, *34*, 522–527. [CrossRef]
41. Di Schino, A.; Barteri, M.; Kenny, J.M. Grain size dependence of mechanical, corrosion and tribological properties of high nitrogen stainless steels. *J. Mater. Sci.* **2003**, *38*, 3257–3262. [CrossRef]
42. Di Schino, A.; Barteri, M.; Kenny, J.M. Effects of grain size on the properties of a low nickel austenitic stainless steel. *J. Mater. Sci.* **2003**, *38*, 4725–4733. [CrossRef]
43. Di Schino, A.; Kenny, J.M. Grain size dependence of the fatigue behaviour of a ultrafine-grained AISI 304 stainless steel. *Mater. Lett.* **2003**, *57*, 3182–3185. [CrossRef]
44. Choi, J.-Y.; Jin, W. Strain induced martensite formation and its effect on strain hardening behavior in the cold drawn 304 austenitic stainless steels. *Scr. Mater.* **1997**, *36*, 99–104. [CrossRef]
45. Lee, S.-J.; Park, Y.-M.; Lee, Y.-K. Reverse transformation mechanism of martensite to austenite in a metastable austenitic alloy. *Mater. Sci. Eng. A* **2009**, *515*, 32–37. [CrossRef]
46. Jung, Y.-S.; Lee, Y.-K.; Matlock, D.K.; Mataya, M.C. Effect of grain size on strain-induced martensitic transformation start temperature in an ultrafine grained metastable austenitic steel. *Met. Mater. Int.* **2011**, *17*, 553–556. [CrossRef]
47. Huang, J.; Ye, X.; Gu, J.; Chen, X.; Xu, Z. Enhanced mechanical properties of type AISI 301LN austenitic stainless steel through advanced thermo mechanical process. *Mater. Sci. Eng. A* **2012**, *532*, 190–195. [CrossRef]
48. Shen, Y.F.; Jia, N.; Wang, Y.D.; Sun, X.; Zuo, L.; Raabe, D. Suppression of twinning and phase transformation in an ultrafine grained 2GPa strong metastable austenitic steel: Experiment and simulation. *Acta Mater.* **2015**, *97*, 305–315. [CrossRef]
49. Gong, N.; Wu, H.; Niu, G.; Zhang, D. Effects of annealing temperature on nano/ultrafine-grained structure in austenite stainless steel. *Mater. Sci. Technol.* **2017**, *33*, 1667–1672. [CrossRef]
50. Gong, N.; Wu, H.-B.; Yu, Z.-C.; Niu, G.; Zhang, D. Studying mechanical properties and micro deformation of ultrafine-grained structures in austenitic stainless steel. *Metals* **2017**, *7*, 188. [CrossRef]
51. Lei, C.; Li, X.; Deng, X.; Wang, Z.; Wang, G. Deformation mechanism and ductile fracture behavior in high strength high ductility nano/ultrafine grained Fe-17Cr-6Ni austenitic steel. *Mater. Sci. Eng. A* **2018**, *709*, 72–81. [CrossRef]
52. Xu, D.M.; Wan, X.L.; Yu, J.X.; Xu, G.; Li, G.Q. Effect of grain refinement on strain hardening and fracture in austenitic stainless steel. *Mater. Sci. Technol.* **2018**, *34*, 1344–1352. [CrossRef]
53. Ravi Kumar, B.; Das, S.K.; Mahato, B.; Ghosh, R.N. Role of strain-induced martensite on microstructural evolution during annealing of metastable austenitic stainless steel. *J. Mater. Sci.* **2010**, *45*, 911–918. [CrossRef]

54. Ravi Kumar, B.; Sharma, S. Recrystallization behavior of a heavily deformed austenitic stainless steel during iterative type annealing. *Metall. Mater. Trans. A* **2014**, *45*, 6027–6038. [CrossRef]
55. Ghosh, S.K.; Mallick, P.; Chattopadhyay, P.P. Effect of reversion of strain induced martensite on microstructure and mechanical properties in an austenitic stainless steel. *J. Mater. Sci.* **2011**, *46*, 3480–3487. [CrossRef]
56. Ghosh, S.K.; Jha, S.; Mallick, P.; Chattopadhyay, P.P. Influence of mechanical deformation and annealing on kinetics of martensite in a stainless steel. *Mater. Manuf. Process.* **2013**, *28*, 249–255. [CrossRef]
57. Mallick, P.; Tewary, N.K.; Ghosh, S.K.; Chattopadhyay, P.P. Microstructure-tensile property correlation in 304 stainless steel after cold deformation and austenite reversion. *Mater. Sci. Eng. A* **2017**, *707*, 488–500. [CrossRef]
58. Mallick, P.; Tewary, N.K.; Ghosh, S.K.; Chattopadhyay, P.P. Effect of TMCP on microstructure and mechanical properties of 304 stainless steel. *Steel Res. Int.* **2018**, *89*, 1800103. [CrossRef]
59. Mallick, P.K. Strain Induced Martensite and its Reversion in 304 Stainless Steel. Ph.D. Thesis, Indian Institute of Engineering Science and Technology, West Bengal, India, 2017.
60. Mateo, A.; Zapata, A.; Fargas, G. Improvement of mechanical properties on metastable stainless steels by reversion heat treatments. *IOP Conf. Ser. Mater. Sci. Eng.* **2013**, *48*, 12001. [CrossRef]
61. Odnobokova, M.; Belyakov, A.; Enikeev, N.; Molodov, D.A.; Kaibyshev, R. Annealing behavior of a 304L stainless steel processed by large strain cold and warm rolling. *Mater. Sci. Eng. A* **2017**, *689*, 370–383. [CrossRef]
62. Shakhova, I.; Dudko, V.; Belyakov, A.; Tsuzaki, K.; Kaibyshev, R. Effect of large strain cold rolling and subsequent annealing on microstructure and mechanical properties of an austenitic stainless steel. *Mater. Sci. Eng. A* **2012**, *545*, 176–186. [CrossRef]
63. Cios, G.; Tokarski, T.; Żywczak, A.; Dziurka, R.; Stępień, M.; Gondek, Ł.; Marciszko, M.; Pawłowski, B.; Wieczerzak, K.; Bała, P. The investigation of strain-induced martensite reverse transformation in AISI 304 austenitic stainless steel. *Metall. Mater. Trans. A* **2017**, *48*, 4999–5008. [CrossRef]
64. Fargas, G.; Zapata, A.; Roa, J.J.; Sapezanskaia, I.; Mateo, A. correlation between microstructure and mechanical properties before and after reversion of metastable austenitic stainless steels. *Metall. Mater. Trans. A* **2015**, *46*, 5697–5707. [CrossRef]
65. Eskandari, M.; Najafizadeh, A.; Kermanpur, A.; Karimi, M. Potential application of nanocrystalline 301 austenitic stainless steel in lightweight vehicle structures. *Mater. Des.* **2009**, *30*, 3869–3872. [CrossRef]
66. Hedayati, A.A.; Najafizadeh, A.; Kermanpur, A.; Forouzan, F. The effect of cold rolling regime on microstructure and mechanical properties of AISI 304L stainless steel. *Mater. Sci. Eng. A* **2010**, *210*, 1017–1023. [CrossRef]
67. Rezaee, A.; Najafizadeh, A.; Kermanpur, A.; Moallemi, M. The influence of reversion annealing behavior on the formation of nanograined structure in AISI 201L austenitic stainless steel through martensite treatment. *Mater. Des.* **2011**, *32*, 4437–4442. [CrossRef]
68. Sadeghpour, S.; Kermanpur, A.; Najafizadeh, A. Influence of Ti microalloying on the formation of nanocrystalline structure in the 201L austenitic stainless steel during martensite thermomechanical treatment. *Mater. Sci. Eng. A* **2013**, *584*, 177–183. [CrossRef]
69. Sadeghpour, S.; Kermanpur, A.; Najafizadeh, A. Formation of nano/ultrafine grain structure in a Ti-modified 201L stainless steel through martensite thermomechanical treatment. *ISIJ Int.* **2014**, *54*, 920–925. [CrossRef]
70. Shirdel, M.; Mirzadeh, H.; Parsa, M.H. Nano/ultrafine grained austenitic stainless steel through the formation and reversion of deformation-induced martensite: Mechanisms, microstructures, mechanical properties, and TRIP effect. *Mater. Charact.* **2015**, *103*, 150–161. [CrossRef]
71. Baghbadorani, H.S.; Kermanpur, A.; Najafizadeh, A.; Behjati, P.; Moallemi, M.; Rezaee, A. Influence of Nb-microalloying on the formation of nano/ultrafine-grained microstructure and mechanical properties during martensite reversion process in a 201-type austenitic stainless steel. *Metall. Mater. Trans. A* **2015**, *46*, 3406–3413. [CrossRef]
72. Rasouli, D.; Kermanpur, A.; Ghassemali, E.; Najafizadeh, A. On the reversion and recrystallization of austenite in the interstitially alloyed Ni-free nano/ultrafine grained austenitic stainless steels. *Met. Mater. Int.* **2019**, *25*, 846–859. [CrossRef]
73. Kheiri, S.; Mirzadeh, H.; Naghizadeh, M. Tailoring the microstructure and mechanical properties of AISI 316L austenitic stainless steel via cold rolling and reversion annealing. *Mater. Sci. Eng. A* **2019**, *759*, 90–96. [CrossRef]

74. Droste, M.; Ullrich, C.; Motylenko, M.; Fleischer, M.; Weidner, A.; Freudenberger, J.; Rafaja, D.; Biermann, H. Fatigue behavior of an ultrafine-grained metastable CrMnNi steel tested under total strain control. *Int. J. Fatigue* **2018**, *106*, 143–152. [CrossRef]
75. Maréchal, D. Linkage between Mechanical Properties and Phase Transformations in a 301LN Austenitic Stainless Steel. Ph.D. Thesis, University of British Columbia, Vancouver, BC, Canada, 2011.
76. Fava, J.; Spinosa, C.; Ruch, M.; Carabedo, F.; Landau, M.; Cosarinsky, G.; Savin, A.; Steigmann, R.; Craus, M.L. Characterization of reverse martensitic transformation in cold-rolled austenitic 316 stainless steel. *Rev. Mater.* **2018**, *23*. [CrossRef]
77. Souza Filho, I.R.; Zilnyk, K.D.; Sandim, M.J.R.; Bolmaro, R.E.; Sandim, H.R.Z. Strain partitioning and texture evolution during cold rolling of AISI 201 austenitic stainless steel. *Mater. Sci. Eng. A* **2017**, *702*, 161–172. [CrossRef]
78. Souza Filho, I.R.; Sandim, M.J.R.; Cohen, R.; Nagamine, L.C.C.M.; Hoffmann, J.; Bolmaro, R.E.; Sandim, H.R.Z. Effects of strain-induced martensite and its reversion on the magnetic properties of AISI 201 austenitic stainless steel. *J. Magn. Magn. Mater.* **2016**, *419*, 156–165. [CrossRef]
79. Souza Filho, I.R.; Junior, D.R.A.; Gauss, C.; Sandim, M.J.R.; Suzuki, P.A.; Sandim, H.R.Z. Austenite reversion in AISI 201 austenitic stainless steel evaluated via in situ synchrotron X-ray diffraction during slow continuous annealing. *Mater. Sci. Eng. A* **2019**, *755*, 267–277. [CrossRef]
80. Hamada, A.S.; Kisko, A.P.; Sahu, P.; Karjalainen, L.P. Enhancement of mechanical properties of a TRIP-aided austenitic stainless steel by controlled reversion annealing. *Mater. Sci. Eng. A* **2015**, *628*, 154–159. [CrossRef]
81. Kisko, A.; Misra, R.D.K.; Talonen, J.; Karjalainen, L.P. The influence of grain size on the strain-induced martensite formation in tensile straining of an austenitic 15Cr–9Mn–Ni–Cu stainless steel. *Mater. Sci. Eng. A* **2013**, *578*, 408–416. [CrossRef]
82. Kisko, A.; Talonen, J.; Porter, D.A.; Karjalainen, L.P. Effect of Nb microalloying on reversion and grain growth in a high-Mn 204Cu austenitic stainless steel. *ISIJ Int.* **2015**, *55*, 2217–2224. [CrossRef]
83. Kisko, A.; Hamada, A.S.; Talonen, J.; Porter, D.; Karjalainen, L.P. Effects of reversion and recrystallization on microstructure and mechanical properties of Nb-alloyed low-Ni high-Mn austenitic stainless steels. *Mater. Sci. Eng. A* **2016**, *657*, 359–370. [CrossRef]
84. Järvenpää, A.; Jaskari, M.; Man, J.; Karjalainen, L.P. Austenite stability in reversion-treated structures of a 301LN steel under tensile loading. *Mater. Charact.* **2017**, *127*, 12–26. [CrossRef]
85. Järvenpää, A.; Jaskari, M.; Man, J.; Karjalainen, L.P. Stability of grain-refined reversed structures in a 301LN austenitic stainless steel under cyclic loading. *Mater. Sci. Eng. A* **2017**, *703*, 280–292. [CrossRef]
86. Järvenpää, A.; Jaskari, M.; Juuti, T.; Karjalainen, P. Demonstrating the effect of precipitation on the mechanical stability of fine-grained austenite in reversion-treated 301LN stainless steel. *Metals* **2017**, *7*, 733. [CrossRef]
87. Järvenpää, A.; Jaskari, M.; Karjalainen, L.P. Properties of induction reversion-refined microstructures of AISI 301LN under monotonic, cyclic and rolling deformation. In *THERMEC 2018*; Trans Tech Publications Ltd.: Stafa-Zurich, Switzerland, 2019; pp. 601–607. [CrossRef]
88. Misra, R.D.K.; Nayak, S.; Venkatasurya, P.K.C.; Ramuni, V.; Somani, M.C.; Karjalainen, L.P. Nanograined/ultrafine-grained structure and tensile deformation behavior of shear phase reversion-induced 301 austenitic stainless steel. *Metall. Mater. Trans. A* **2010**, *41*, 2162–2174. [CrossRef]
89. Rajasekhara, S.; Ferreira, P.J.; Karjalainen, L.P.; Kyrolainen, A. Microstructure evolution in nano/sub-micron grained AISI 301 stainless steel. In Proceedings of the 6th European Congress Stainless Steel Science and Market, Helsinki, Finland, 10–13 June 2008.
90. Misra, R.D.K.; Kumar, B.R.; Somani, M.; Karjalainen, P. Deformation processes during tensile straining of ultrafine/nanograined structures formed by reversion in metastable austenitic steels. *Scr. Mater.* **2008**, *59*, 79–82. [CrossRef]
91. Misra, R.D.K.; Nayak, S.; Mali, S.A.; Shah, J.S.; Somani, M.C.; Karjalainen, L.P. On the significance of nature of strain-induced martensite on phase-reversion-induced nanograined/ultrafine-grained austenitic stainless steel. *Metall. Mater. Trans. A* **2010**, *41*, 3–10. [CrossRef]
92. Misra, R.D.K.; Zhang, Z.; Venkatasurya, P.K.C.; Somani, M.C.; Karjalainen, L.P. Martensite shear phase reversion-induced nanograined/ultrafine-grained Fe–16Cr–10Ni alloy: The effect of interstitial alloying elements and degree of austenite stability on phase reversion. *Mater. Sci. Eng. A* **2010**, *527*, 7779–7792. [CrossRef]

93. Misra, R.D.K.; Zhang, Z.; Jia, Z.; Surya, P.K.C.V.; Somani, M.C.; Karjalainen, L.P. Nanomechanical insights into the deformation behavior of austenitic alloys with different stacking fault energies and austenitic stability. *Mater. Sci. Eng. A* **2011**, *528*, 6958–6963. [CrossRef]
94. Challa, V.S.A.; Wan, X.L.; Somani, M.C.; Karjalainen, L.P.; Misra, R.D.K. Strain hardening behavior of phase reversion-induced nanograined/ultrafine-grained (NG/UFG) austenitic stainless steel and relationship with grain size and deformation mechanism. *Mater. Sci. Eng. A* **2014**, *613*, 60–70. [CrossRef]
95. Challa, V.S.A.; Wan, X.L.; Somani, M.C.; Karjalainen, L.P.; Misra, R.D.K. Significance of interplay between austenite stability and deformation mechanisms in governing three-stage work hardening behavior of phase-reversion induced nanograined/ultrafine-grained (NG/UFG) stainless steels with high strength-high ductility combination. *Scr. Mater.* **2014**, *86*, 60–63. [CrossRef]
96. Challa, V.S.A.; Misra, R.D.K.; Somani, M.C.; Wang, Z.D. Strain hardening behavior of nanograined/ultrafine-grained (NG/UFG) austenitic 16Cr–10Ni stainless steel and its relationship to austenite stability and deformation behavior. *Mater. Sci. Eng. A* **2016**, *649*, 153–157. [CrossRef]
97. Misra, R.D.K.; Injeti, V.S.Y.; Somani, M.C. The significance of deformation mechanisms on the fracture behavior of phase reversion-induced nanostructured austenitic stainless steel. *Sci. Rep.* **2018**, *8*, 7908. [CrossRef]
98. Chlupová, A.; Man, J.; Polák, J.; Karjalainen, L.P. Microstructural investigation and mechanical testing of an ultrafine-grained austenitic stainless steel. In *NANOCON 2013*; Tanger Ltd.: Ostrava, Czech Republic, 2013; pp. 733–738.
99. Chlupová, A.; Man, J.; Kuběna, I.; Polák, J.; Karjalainen, L.P. LCF behaviour of ultrafine grained 301LN stainless steel. *Procedia Eng.* **2014**, *74*, 147–150. [CrossRef]
100. Man, J.; Kuběna, I.; Smaga, M.; Man, O.; Järvenpää, A.; Weidner, A.; Chlup, Z.; Polák, J. Microstructural changes during deformation of AISI 300 grade austenitic stainless steels: Impact of chemical heterogeneity. *Procedia Struct. Integr.* **2016**, *2*, 2299–2306. [CrossRef]
101. Kisko, A. Microstructure and Properties of Reversion Treated Low-Ni High-Mn Austenitic Stainless Steels. Ph.D. Thesis, University of Oulu, Oulu, Finland, 2016; ISSN 1796-2226.
102. Järvenpää, A. Microstructures, Mechanical Stability and Strength of Low-Temperature AISILN Stainless steel Under Monotonic and Dynamic Loading. Ph.D. Thesis, University of Oulu, Oulu, Finland, 2019; ISSN 1796-2226.
103. Järvenpää, A.; Karjalainen, L.P. An overview of mechanical properties of today's grain-refined austenitic stainless steels. In Proceedings of the ESSC & DUPLEX, ASMET, Vienna, Austria, 31 September–2 October 2019; pp. 12–21.
104. Komatsuseiki Kosakusho Co., Ltd. Available online: https://www.komatsuseiki.co.jp/english/future/03.php (accessed on 9 August 2016).
105. Komatsu, T.; Matsumura, T.; Torizuka, S. Effect of grain size in stainless steel on cutting performance in micro-scale cutting. *Int. J. Autom. Technol.* **2011**, *5*, 334–341. [CrossRef]
106. Komatsu, T.; Kobayashi, H.; Torizuka, S.; Nagayama, S. Micro hole piercing for ultra fine grained steel. In *THERMEC 2013*; Trans Tech Publications Ltd.: Stafa-Zurich, Switzerland, 2014; Volume 783, pp. 2653–2658. [CrossRef]
107. Komatsu, T.; Yoshino, T.; Matsumura, T.; Torizuka, S. Effect of crystal grain size in stainless steel on cutting process in micromilling. *Procedia CIRP* **2012**, *1*, 150–155. [CrossRef]
108. Nippon Steel & Sumitomo Metal Product Catalog: SUS304 BA1. Available online: https://stainless.nipponsteel.com/product/grade/nssmc_series/product/sus304_ba1.php (accessed on 6 December 2019).
109. Nippon Steel & Sumitomo Metal Product Catalog: NSSMC-NAR-301L BA1. Available online: https://stainless.nipponsteel.com/product/grade/nssmc_series/product/nssmc-nar-301l_ba1.php (accessed on 6 December 2019).
110. Lo, K.H.; Shek, C.H.; Lai, J.K.L. Recent developments in stainless steels. *Mater. Sci. Eng. R* **2009**, *65*, 39–104. [CrossRef]
111. Pereloma, E.; Gazder, A.; Timokhina, I. Retained austenite: Transformation-induced plasticity. *Encycl. Iron Steel Alloys* **2016**, 3088–3103. [CrossRef]
112. Beese, A.M.; Mohr, D. Effect of stress triaxiality and Lode angle on the kinetics of strain-induced austenite-to-martensite transformation. *Acta Mater.* **2011**, *59*, 2589–2600. [CrossRef]
113. Das, A.; Tarafder, S.; Chakraborti, P.C. Estimation of deformation induced martensite in austenitic stainless steels. *Mater. Sci. Eng. A* **2011**, *529*, 9–20. [CrossRef]

114. Nohara, K.; Ono, Y.; Ohashi, N. Composition and grain size dependencies of strain-induced martensitic transformation in metastable austenitic stainless steels. *ISIJ Int.* **1977**, *63*, 772–782. [CrossRef]
115. Noh, H.-S.; Kang, J.-H.; Kim, K.-M.; Kim, S.-J. Different effects of Ni and Mn on thermodynamic and mechanical stabilities in Cr-Ni-Mn austenitic steels. *Metall. Mater. Trans. A* **2019**, *50*, 616–624. [CrossRef]
116. Furukane, S.; Torizuka, S. Effect of grain size and dislocation density on strain-induced martensitic transformation in austenitic stainless steels. *Tetsu Hagane* **2019**, *105*, 827–836. [CrossRef]
117. Roy, B.; Kumar, R.; Das, J. Effect of cryorolling on the microstructure and tensile properties of bulk nano-austenitic stainless steel. *Mater. Sci. Eng. A* **2015**, *631*, 241–247. [CrossRef]
118. Xiong, Y.; He, T.; Wang, J.; Lu, Y.; Chen, L.; Ren, F.; Liu, Y.; Volinsky, A.A. Cryorolling effect on microstructure and mechanical properties of Fe–25Cr–20Ni austenitic stainless steel. *Mater. Des.* **2015**, *88*, 398–405. [CrossRef]
119. Zheng, C.; Liu, C.; Ren, M.; Jiang, H.; Li, L. Microstructure and mechanical behavior of an AISI 304 austenitic stainless steel prepared by cold- or cryogenic-rolling and annealing. *Mater. Sci. Eng. A* **2018**, *724*, 260–268. [CrossRef]
120. Mallick, P.; Tewary, N.K.; Ghosh, S.K.; Chattopadhyay, P.P. Effect of cryogenic deformation on microstructure and mechanical properties of 304 austenitic stainless steel. *Mater. Charact.* **2017**, *133*, 77–86. [CrossRef]
121. Martins, L.F.M.; Plaut, R.L.; Padilha, A.F. Effect of carbon on the cold-worked state and annealing behavior of two 18wt%Cr-8wt%Ni austenitic stainless steels. *ISIJ Int.* **1998**, *38*, 572–579. [CrossRef]
122. Mirzadeh, H.; Najafizadeh, A. Correlation between processing parameters and strain-induced martensitic transformation in cold worked AISI 301 stainless steel. *Mater. Charact.* **2008**, *59*, 1650–1654. [CrossRef]
123. Xu, D.; Wan, X.; Yu, J.; Xu, G.; Li, G. Effect of cold deformation on microstructures and mechanical properties of austenitic stainless steel. *Metals* **2018**, *8*, 522. [CrossRef]
124. Ahmedabadi, P.M.; Kain, V.; Agrawal, A. Modelling kinetics of strain-induced martensite transformation during plastic deformation of austenitic stainless steel. *Mater. Des.* **2016**, *109*, 466–475. [CrossRef]
125. Niessen, F. Phase Transformations in Supermartensitic Stainless Steels. Ph.D. Thesis, Technical University of Denmark, Lyngby, Denmark, 2018.
126. Yang, D.P.; Wu, D.; Yi, H.L. Reverse transformation from martensite into austenite in a medium-Mn steel. *Scr. Mater.* **2019**, *161*, 1–5. [CrossRef]
127. Santos, T.F.A.; Andrade, M.S. Avaliação dilatométrica da reversão das martensitas induzidas por deformação em um aço inoxidável austenítico do tipo ABNT 304. *Matéria* **2008**, *13*, 587–596. [CrossRef]
128. Santos, T.F.A.; Andrade, M.S. Internal friction on AISI 304 stainless steels with low tensile deformations at temperatures between 50 and 20 °C. *Adv. Mater. Sci. Eng.* **2010**, *2010*, 326736. [CrossRef]
129. Dryzek, E.; Sarnek, M.; Wróbel, M. Reverse transformation of deformation-induced martensite in austenitic stainless steel studied by positron annihilation. *J. Mater. Sci.* **2014**, *49*, 8449–8458. [CrossRef]
130. Knutsson, A.; Hedström, P.; Odén, M. Reverse martensitic transformation and resulting microstructure in a cold rolled metastable austenitic stainless steel. *Steel Res. Int.* **2008**, *79*, 433–439. [CrossRef]
131. Talonen, J.; Aspegren, P.; Hänninen, H. Comparison of different methods for measuring strain induced α-martensite content in austenitic steels. *Mater. Sci. Technol.* **2004**, *20*, 1506–1512. [CrossRef]
132. Cios, G.; Tokarski, T.; Bała, P. Strain-induced martensite reversion in 18Cr–8Ni steel – transmission Kikuchi diffraction study. *Mater. Sci. Technol.* **2018**, *34*, 580–583. [CrossRef]
133. Wei, S.; Jiang, M.; Tasan, C.C. Interstitial-free bake hardening realized by epsilon martensite reverse transformation. *Metall. Mater. Trans. A* **2019**, *50*, 3985–3991. [CrossRef]
134. Yagodzinsky, Y.; Saukkonen, T.; Romu, J.; Hänninen, H. Comparative study of nitrogen and carbon effects on mechanism of reversion of a'-martensite to austenite in metastable AISI 301 steel grades. In Proceedings of the International Conference on High Nitrogen Steels, Jiuzhaigou Valley, China, 29–31 August 2006; pp. 59–66.
135. Johannsen, D.L.; Kyrolainen, A.; Ferreira, P.J. Influence of annealing treatment on the formation of nano/submicron grain size AISI 301 austenitic stainless steels. *Metall. Mater. Trans. A* **2006**, *37*, 2325–2338. [CrossRef]
136. Rajasekhara, S.; Ferreira, P.J. Martensite—Austenite phase transformation kinetics in an ultrafine-grained metastable austenitic stainless steel. *Acta Mater.* **2011**, *59*, 738–748. [CrossRef]

137. Sun, G.S.; Du, L.X.; Hu, J.; Xie, H.; Wu, H.Y.; Misra, R.D.K. Ultrahigh strength nano/ultrafine-grained 304 stainless steel through three-stage cold rolling and annealing treatment. *Mater. Charact.* **2015**, *110*, 228–235. [CrossRef]
138. Padilha, A.F.; Plaut, R.L.; Rios, P.R. Annealing of cold-worked austenitic stainless steels. *ISIJ Int.* **2003**, *43*, 135–143. [CrossRef]
139. Haessner, F.; Plaut, R.L.; Padilha, A.F. Separation of static recrystallization and reverse transformation of deformation-induced martensite in an austenitic stainless steel by calorimetric measurements. *ISIJ Int.* **2003**, *43*, 1472–1474. [CrossRef]
140. Sun, G.S.; Du, L.X.; Hu, J.; Misra, R.D.K. Microstructural evolution and recrystallization behavior of cold rolled austenitic stainless steel with dual phase microstructure during isothermal annealing. *Mater. Sci. Eng. A* **2018**, *709*, 254–264. [CrossRef]
141. Apple, C.A.; Krauss, G. The effect of heating rate on the martensite to austenite transformation in Fe-Ni-C alloys. *Acta Metall.* **1972**, *20*, 849–856. [CrossRef]
142. Sun, G.S.; Du, L.X.; Hu, J.; Xie, H.; Misra, R.D.K. Low temperature superplastic-like deformation and fracture behavior of nano/ultrafine-grained metastable austenitic stainless steel. *Mater. Des.* **2017**, *117*, 223–231. [CrossRef]
143. Mumtaz, K.; Takahashi, S.; Echigoya, J.; Kamada, Y.; Zhang, L.F.; Kikuchi, H.; Ara, K.; Sato, M. Magnetic measurements of the reverse martensite to austenite transformation in a rolled austenitic stainless steel. *J. Mater. Sci.* **2004**, *39*, 1997–2010. [CrossRef]
144. Tavares, S.S.M.; da Silva, M.R.; Neto, J.M.; Miraglia, S.; Fruchart, D. Ferromagnetic properties of cold rolled AISI 304L steel. *J. Magn. Magn. Mater.* **2002**, *242–245*, 1391–1394. [CrossRef]
145. Behjati, P.; Kermanpur, A.; Karjalainen, L.P.; Järvenpää, A.; Jaskari, M.; Samaei Baghbadorani, H.; Najafizadeh, A.; Hamada, A. Influence of prior cold rolling reduction on microstructure and mechanical properties of a reversion annealed high-Mn austenitic steel. *Mater. Sci. Eng. A* **2016**, *650*, 119–128. [CrossRef]
146. Ravi Kumar, B.; Sharma, S.; Mahato, B. Formation of ultrafine grained microstructure in the austenitic stainless steel and its impact on tensile properties. *Mater. Sci. Eng. A* **2011**, *528*, 2209–2216. [CrossRef]
147. Ravi Kumar, B.; Mahato, B.; Sharma, S.; Sahu, J.K. Effect of cyclic thermal process on ultrafine grain formation in AISI 304L austenitic stainless steel. *Metall. Mater. Trans. A* **2009**, *40*, 3226–3234. [CrossRef]
148. Ravi Kumar, B.; Raabe, D. Tensile deformation characteristics of bulk ultrafine-grained austenitic stainless steel produced by thermal cycling. *Scr. Mater.* **2012**, *66*, 634–637. [CrossRef]
149. Xu, D.M.; Li, G.Q.; Wan, X.L.; Misra, R.D.K.; Yu, J.X.; Xu, G. On the deformation mechanism of austenitic stainless steel at elevated temperatures: A critical analysis of fine-grained versus coarse-grained structure. *Mater. Sci. Eng. A* **2019**. [CrossRef]
150. Lehto, P.; Remes, H.; Saukkonen, T.; Hänninen, H.; Romanoff, J. Influence of grain size distribution on the Hall–Petch relationship of welded structural steel. *Mater. Sci. Eng. A* **2014**, *592*, 28–39. [CrossRef]
151. *Technical Data for Annealed 301LN*; Outokumpu Stainless Oy: Helsinki, Finland, 2016.
152. Bleck, W.; Guo, X.; Ma, Y. The TRIP effect and its application in cold formable sheet steels. *Steel Res. Int.* **2017**, *88*, 1700218. [CrossRef]
153. Guo, X.; Post, J.; Groen, M.; Bleck, W. Stress oriented delayed cracking induced by dynamic martensitic transformation in meta-stable austenitic stainless steels. *Steel Res. Int.* **2011**, *82*, 6–13. [CrossRef]
154. Weiß, A.; Gutte, H.; Scheller, P.R. Deformation induced martensite formation and its effect on transformation induced plasticity (TRIP). *Steel Res. Int.* **2006**, *77*, 727–732. [CrossRef]
155. Talonen, J. Effect of Strain-Induced α′-Martensite Transformation on Mechanical Properties of Metastable Austenitic Stainless Steels. Ph.D. Thesis, TKK Dissertations 71, Espoo, Finland, 2007.
156. Hamada, A.S.; Karjalainen, L.P.; Misra, R.D.K.; Talonen, J. Contribution of deformation mechanisms to strength and ductility in two Cr–Mn grade austenitic stainless steels. *Mater. Sci. Eng. A* **2013**, *559*, 336–344. [CrossRef]
157. Olson, G.B.; Cohen, M. Kinetics of strain-induced martensitic nucleation. *Metall. Trans. A* **1975**, *6*, 791. [CrossRef]
158. Lichtenfeld, J.A.; Van Tyne, C.J.; Mataya, M.C. Effect of strain rate on stress-strain behavior of alloy 309 and 304L austenitic stainless steel. *Metall. Mater. Trans. A* **2006**, *37*, 147–161. [CrossRef]
159. Yoo, C.-S.; Park, Y.-M.; Jung, Y.-S.; Lee, Y.-K. Effect of grain size on transformation-induced plasticity in an ultrafine-grained metastable austenitic steel. *Scr. Mater.* **2008**, *59*, 71–74. [CrossRef]

160. Matsuoka, Y.; Iwasaki, T.; Nakada, N.; Tsuchiyama, T.; Takaki, S. Effect of grain size on thermal and mechanical stability of austenite in metastable austenitic stainless steel. *ISIJ Int.* **2013**, *53*, 1224–1230. [CrossRef]
161. Ravi Kumar, B.; Gujral, A. Plastic deformation modes in mono- and bimodal-type ultrafine-grained austenitic stainless steel. *Metallogr. Microstruct. Anal.* **2014**, *3*, 397–407. [CrossRef]
162. Lee, Y.K.; Jin, J.E.; Ma, Y.Q. Transformation-induced extraordinary ductility in an ultrafine-grained alloy with nanosized precipitates. *Scr. Mater.* **2007**, *57*, 707–710. [CrossRef]
163. He, Y.M.; Wang, Y.H.; Guo, K.; Wang, T.S. Effect of carbide precipitation on strain-hardening behavior and deformation mechanism of metastable austenitic stainless steel after repetitive cold rolling and reversion annealing. *Mater. Sci. Eng. A* **2017**, *708*, 248–253. [CrossRef]
164. Saenarjhan, N.; Kang, J.-H.; Kim, S.-J. Effects of carbon and nitrogen on austenite stability and tensile deformation behavior of 15Cr-15Mn-4Ni based austenitic stainless steels. *Mater. Sci. Eng. A* **2019**, *742*, 608–616. [CrossRef]
165. Kim, K.-S.; Kang, J.-H.; Kim, S.-J. Effects of carbon and nitrogen on precipitation and tensile behavior in 15Cr-15Mn-4Ni austenitic stainless steels. *Mater. Sci. Eng. A* **2018**, *712*, 114–121. [CrossRef]
166. Karimi, M.; Najafizadeh, A.; Kermanpur, A.; Eskandari, M. Effect of martensite to austenite reversion on the formation of nano/submicron grained AISI 301 stainless steel. *Mater. Charact.* **2009**, *60*, 1220–1223. [CrossRef]
167. Hong, S.-M.; Kim, M.-Y.; Min, D.-J.; Lee, K.; Shim, J.-H.; Kim, D.-I.; Suh, J.-Y.; Jung, W.-S.; Choi, I.-S. Unraveling the origin of strain-induced precipitation of M23C6 in the plastically deformed 347 austenite stainless steel. *Mater. Charact.* **2014**, *94*, 7–13. [CrossRef]
168. Allain, S.; Chateau, J.-P.; Bouaziz, O.; Migot, S.; Guelton, N. Correlations between the calculated stacking fault energy and the plasticity mechanisms in Fe–Mn–C alloys. *Mater. Sci. Eng. A* **2004**, *387–389*, 158–162. [CrossRef]
169. Saeed-Akbari, A.; Imlau, J.; Prahl, U.; Bleck, W. Derivation and variation in composition-dependent stacking fault energy maps based on subregular solution model in high-manganese steels. *Metall. Mater. Trans. A* **2009**, *40*, 3076–3090. [CrossRef]
170. Lee, S.; Shin, S.; Kwon, M.; Lee, K.; De Cooman, B.C. Tensile properties of medium Mn steel with a bimodal UFG $\alpha + \gamma$ and coarse δ-ferrite microstructure. *Metall. Mater. Trans. A* **2017**, *48*, 1678–1700. [CrossRef]
171. Misra, R.D.K.; Challa, V.S.A.; Venkatsurya, P.K.C.; Shen, Y.F.; Somani, M.C.; Karjalainen, L.P. Interplay between grain structure, deformation mechanisms and austenite stability in phase-reversion-induced nanograined/ultrafine-grained austenitic ferrous alloy. *Acta Mater.* **2015**, *84*, 339–348. [CrossRef]
172. Mahato, B.; Shee, S.K.; Sahu, T.; Chowdhury, S.G.; Sahu, P.; Porter, D.A.; Karjalainen, L.P. An effective stacking fault energy viewpoint on the formation of extended defects and their contribution to strain hardening in a Fe–Mn–Si–Al twinning-induced plasticity steel. *Acta Mater.* **2015**, *86*, 69–79. [CrossRef]
173. Gao, S.; Bai, Y.; Zheng, R.; Tian, Y.; Mao, W.; Shibata, A.; Tsuji, N. Mechanism of huge Lüders-type deformation in ultrafine grained austenitic stainless steel. *Scr. Mater.* **2019**, *159*, 28–32. [CrossRef]
174. Song, R.; Ponge, D.; Raabe, D. Mechanical properties of an ultrafine grained C–Mn steel processed by warm deformation and annealing. *Acta Mater.* **2005**, *53*, 4881–4892. [CrossRef]
175. Song, R.; Ponge, D.; Raabe, D.; Speer, J.G.; Matlock, D.K. Overview of processing, microstructure and mechanical properties of ultrafine grained bcc steels. *Mater. Sci. Eng. A* **2006**, *441*, 1–17. [CrossRef]
176. Lee, T.; Park, C.H.; Lee, D.-L.; Lee, C.S. Enhancing tensile properties of ultrafine-grained medium-carbon steel utilizing fine carbides. *Mater. Sci. Eng. A* **2011**, *528*, 6558–6564. [CrossRef]
177. Dini, G.; Najafizadeh, A.; Ueji, R.; Monir-Vaghefi, S.M. Tensile deformation behavior of high manganese austenitic steel: The role of grain size. *Mater. Des.* **2010**, *31*, 3395–3402. [CrossRef]
178. Mao, Q.; Gao, B.; Li, J.; Huang, Z.; Li, Y. Enhanced tensile properties of 316L steel via grain refinement and low-strain rolling. *Mater. Sci. Technol.* **2019**, *35*, 1497–1503. [CrossRef]
179. Jung, Y.-S.; Lee, Y.-K. Effect of pre-deformation on the tensile properties of a metastable austenitic steel. *Scr. Mater.* **2008**, *59*, 47–50. [CrossRef]
180. Höppel, H.W.; Kautz, M.; Xu, C.; Murashkin, M.; Langdon, T.G.; Valiev, R.Z.; Mughrabi, H. An overview: Fatigue behaviour of ultrafine-grained metals and alloys. *Int. J. Fatigue* **2006**, *28*, 1001–1010. [CrossRef]
181. Ueno, H.; Kakihata, K.; Kaneko, Y.; Hashimoto, S.; Vinogradov, A. Enhanced fatigue properties of nanostructured austenitic SUS 316L stainless steel. *Acta Mater.* **2011**, *59*, 7060–7069. [CrossRef]
182. Liu, J.; Deng, X.T.; Huang, L.; Wang, Z.D. High-cycle fatigue behavior of 18Cr-8Ni austenitic stainless steels with grains ranging from nano/ultrafine-size to coarse. *Mater. Sci. Eng. A* **2018**, *733*, 128–136. [CrossRef]

183. Järvenpää, A.; Karjalainen, L.P.; Jaskari, M. Effect of grain size on fatigue behavior of Type 301LN stainless steel. *Int. J. Fatigue* **2014**, *65*. [CrossRef]
184. Man, J.; Chlupová, A.; Kuběna, I.; Kruml, T.; Man, O.; Polak, J. LCF Behaviour of 301LN steel: Coarse-grained vs. UFG-bimodal structure. In Proceedings of the LCF8, the Eighth International Conference on Low Cycle Fatigue, Dresden, Germany, 27–29 June 2017; pp. 27–29.
185. Uusitalo, J.; Karjalainen, L.P.; Retraint, D.; Palosaari, M. Fatigue properties of steels with ultrasonic attrition treated surface layers. *Mater. Sci. Forum* **2009**, *604–605*, 239–248. [CrossRef]
186. Biermann, H.; Glage, A.; Droste, M. Influence of temperature on fatigue-induced martensitic phase transformation in a metastable CrMnNi-steel. *Metall. Mater. Trans. A* **2016**, *47*, 84–94. [CrossRef]
187. Glage, A.; Weidner, A.; Biermann, H. Effect of austenite stability on the low cycle fatigue behavior and microstructure of high alloyed metastable austenitic cast TRIP steels. *Procedia Eng.* **2010**, *2*, 2085–2094. [CrossRef]
188. Glage, A.; Weidner, A.; Biermann, H. Cyclic deformation behaviour of three austenitic cast CrMnNi TRIP/TWIP steels with various Ni content. *Steel Res. Int.* **2011**, *82*, 1040–1047. [CrossRef]
189. Hennessy, D.; Steckel, G.; Altstetter, C. Phase transformation of stainless steel during fatigue. *Metall. Trans. A* **1976**, *7*, 415–424. [CrossRef]
190. Mateo, A.; Fargas, G.; Zapata, A. Martensitic transformation during fatigue testing of an AISI 301LN stainless steel. *IOP Conf. Ser. Mater. Sci. Eng.* **2012**, *31*, 12010. [CrossRef]
191. Topic, M.; Tait, R.B.; Allen, C. The fatigue behaviour of metastable (AISI-304) austenitic stainless steel wires. *Int. J. Fatigue* **2007**, *29*, 656–665. [CrossRef]
192. Smaga, M.; Walther, F.; Eifler, D. Deformation-induced martensitic transformation in metastable austenitic steels. *Mater. Sci. Eng. A* **2008**, *483–484*, 394–397. [CrossRef]
193. Droste, M.; Järvenpää, A.; Jaskari, M.; Motylenko, M.; Weidner, A.; Karjalainen, L.P.; Biermann, H. The role of grain size in the cyclic deformation behavior of laser reversion annealed high-alloy TRIP steel. *Fatigue Fract. Eng. Mater. Struct.* **2020**. in preparation.
194. Hamada, A.S.; Karjalainen, L.P.; Surya, P.K.C.V.; Misra, R.D.K. Fatigue behavior of ultrafine-grained and coarse-grained Cr–Ni austenitic stainless steels. *Mater. Sci. Eng. A* **2011**, *528*, 3890–3896. [CrossRef]
195. Poulon, A.; Brochet, S.; Glez, J.-C.; Mithieux, J.-D.; Vogt, J.-B. Influence of texture and grain size on martensitic transformations occurring during low-cycle fatigue of a fine-grained austenitic stainless steel. *Adv. Eng. Mater.* **2010**, *12*, 1041–1046. [CrossRef]
196. Man, J.; Järvenpää, A.; Jaskari, M.; Kuběna, I.; Fintová, S.; Chlupová, A.; Karjalainen, L.P.; Polák, J. Cyclic deformation behaviour and stability of grain-refined 301LN austenitic stainless structure. *MATEC Web Conf.* **2018**, *165*. [CrossRef]
197. Hamada, A.S.; Järvenpää, A.; Ahmed, E.; Sahu, P.; Farahat, A.I.Z. Enhancement in grain-structure and mechanical properties of laser reversion treated metastable austenitic stainless steel. *Mater. Des.* **2016**, *94*, 345–352. [CrossRef]
198. Järvenpää, A.; Jaskari, M.; Mäntyjärvi, K.; Karjalainen, P. Comparison of the formability of austenitic reversion-treated and temper-rolled 17Cr-7Ni steels. In Proceedings of the ESAFORM19 Conference, Vitoria-Gasteiz, Austria, 8–10 May 2019. [CrossRef]
199. Järvenpää, A.; Jaskari, M.; Keskitalo, M.; Mäntyjärvi, K.; Karjalainen, P. Microstructure and mechanical properties of laser-welded high-strength AISI 301LN steel in reversion-treated and temper-rolled conditions. *Procedia Manuf.* **2019**, *36*, 216–223. [CrossRef]
200. Karjalainen, P.; Oikarinen, T.; Somani, M.; Kyröläinen, A. Softening of temper-rolled austenitic stainless steels in welding. In Proceedings of the Fifteenth International Conference & Exhibition on the Joining of Materials, Helsingor, Denmark, 3–6 May 2009.
201. Cvetkovski, S.; Karjalainen, L.P.; Kujanpää, V.; Ahmad, A. Estimation of heat input in TIG and laser welding of stainless steel sheet. In Proceedings of the IIW International Conference on Advances in Welding and Allied Technologies, Singapore, Singapore, 16–17 July 2009; pp. 323–328.
202. Cvetkovski, S.; Karjalainen, L.P.; Kisko, A.; Lantto, S. Characteristic microstructures in simulated HAZ of temper rolled austenitic stainless steel EN 1.4318. In Proceedings of the 7th European Stainless Steel Conference—Science and Market, Como, Italy, 21–23 September 2011.
203. Lv, Y.; Luo, H.; Tang, J.; Guo, J.; Pi, J.; Ye, K. Corrosion properties of phase reversion induced nano/ultrafine grained AISI 304 metastable austenite stainless steel. *Mater. Res. Bull.* **2018**, *107*, 421–429. [CrossRef]

204. Han, J.; Wang, Z.; Jiang, L. Properties of a 304 Austenitic stainless steel hot strip by TMCP. *J. Iron Steel Res. Int.* **2007**, *14*, 282–287. [CrossRef]
205. Hamada, A.S.; Karjalainen, L.P.; Somani, M.C. Electrochemical corrosion behaviour of a novel submicron-grained austenitic stainless steel in an acidic NaCl solution. *Mater. Sci. Eng. A* **2006**, *431*, 211–217. [CrossRef]
206. Misra, R.D.K.; Girase, B.; Venkata Surya, P.K.C.; Somani, M.C.; Karjalainen, L.P. Cellular mechanisms of enhanced osteoblasts functions via phase-reversion induced nano/submicron-grained structure in a low-Ni austenitic stainless steel. *Adv. Eng. Mater.* **2011**, *13*, B483–B492. [CrossRef]
207. Venkatsurya, P.K.C.; Thein-Han, W.W.; Misra, R.D.K.; Somani, M.C.; Karjalainen, L.P. Advancing nanograined/ultrafine-grained structures for metal implant technology: Interplay between grooving of nano/ultrafine grains and cellular response. *Mater. Sci. Eng. C* **2010**, *30*, 1050–1059. [CrossRef]
208. Nune, C.; Misra, R.D.K. Impact of grain structure of austenitic stainless steel on osteoblasts differention and mineralisation. *Mater. Technol.* **2015**, *30*, 76–85. [CrossRef]
209. Misra, R.D.K.; Nune, C.; Pesacreta, T.C.; Somani, M.C.; Karjalainen, L.P. Understanding the impact of grain structure in austenitic stainless steel from a nanograined regime to a coarse-grained regime on osteoblast functions using a novel metal deformation–annealing sequence. *Acta Biomater.* **2013**, *9*, 6245–6258. [CrossRef] [PubMed]
210. Nune, C.; Misra, R.D.K.; Somani, M.C.; Karjalainen, L.P. Dependence of cellular activity at protein adsorbed biointerfaces with nano- to microscale dimensionality. *J. Biomed. Mater. Res. Part A* **2014**, *102*, 1663–1676. [CrossRef] [PubMed]
211. Gong, N.; Hu, C.; Hu, B.; An, B.; Misra, R.D.K. On the mechanical behavior of austenitic stainless steel with nano/ultrafine grains and comparison with micrometer austenitic grains counterpart and their biological functions. *J. Mech. Behav. Biomed. Mater.* **2020**, *101*, 103433. [CrossRef] [PubMed]
212. Tufan, Y.; Demir, E.C.; Efe, M.; Ercan, B. Efficient fabrication of ultrafine-grained 316L stainless steel surfaces for orthopaedic applications. *Mater. Sci. Technol.* **2019**, *35*, 1891–1897. [CrossRef]
213. Luo, F.; Tang, Z.; Xiao, S.; Xiang, Y. Study on properties of copper-containing austenitic antibacterial stainless steel. *Mater. Technol.* **2019**, *34*, 525–533. [CrossRef]
214. Hong, I.T.; Koo, C.H. Antibacterial properties, corrosion resistance and mechanical properties of Cu-modified SUS 304 stainless steel. *Mater. Sci. Eng. A* **2005**, *393*, 213–322. [CrossRef]
215. Lü, Y.; Hutchinson, B.; Molodov, D.A.; Gottstein, G. Effect of deformation and annealing on the formation and reversion of ε-martensite in an Fe–Mn–C alloy. *Acta Mater.* **2010**, *58*, 3079–3090. [CrossRef]
216. Berrenberg, F.; Haase, C.; Barrales-Mora, L.A.; Molodov, D.A. Enhancement of the strength-ductility combination of twinning-induced/transformation-induced plasticity steels by reversion annealing. *Mater. Sci. Eng. A* **2017**, *681*, 56–64. [CrossRef]
217. Escobar, D.P.; Dafé, S.S.F.; Santos, D.B. Martensite reversion and texture formation in 17Mn-0.06C TRIP/TWIP steel after hot cold rolling and annealing. *J. Mater. Res. Technol.* **2015**, *4*, 162–170. [CrossRef]
218. Dastur, P.; Zarei-Hanzaki, A.; Pishbin, M.H.; Moallemi, M.; Abedi, H.R. Transformation and twinning induced plasticity in an advanced high Mn austenitic steel processed by martensite reversion treatment. *Mater. Sci. Eng. A* **2017**, *696*, 511–519. [CrossRef]
219. Dastur, P.; Zarei-Hanzaki, A.; Rahimi, R.; Moallemi, M.; Klemm, V.; De Cooman, B.C.; Mola, J. Martensite reversion duality behavior in a cold-rolled high Mn transformation-induced plasticity steel. *J. Metall. Mater. Trans. A* **2019**, *50A*, 4550–4560. [CrossRef]
220. Souza Filho, I.R.; Kwiatkowski Da Silva, A.; Sandim, M.J.R.; Ponge, D.; Gault, B.; Sandim, H.R.Z.; Raabe, D. Martensite to austenite reversion in a high-Mn steel: Partitioning- dependent two-stage kinetics revealed by atom probe tomography, in-situ magnetic measurements and simulation. *Acta Mater.* **2019**, *166*, 178–191. [CrossRef]
221. Mohammad-Ebrahimi, M.H.; Zarei-Hanzaki, A.; Abedi, H.R.; Vakili, S.M.; Soundararajan, C.K. The enhanced static recrystallization kinetics of a non-equiatomic high entropy alloy through the reverse transformation of strain induced martensite. *J. Alloys Compd.* **2019**, *806*, 1550–1563. [CrossRef]